ESA CONTRACT REPORT

Contract Report to the European Space Agency

Support-to-Science-Element (STSE) Study
EarthCARE Assimilation

WP-3100 report: Data monitoring experiments for radar and lidar

August 2013, updated February 2014

Authors: S. Di Michele and M. Janisková

ESA ESTEC contract 4000102816/11/NL/CT

European Centre for Medium-Range Weather Forecasts
Europäisches Zentrum für mittelfristige Wettervorhersage
Centre européen pour les prévisions météorologiques à moyen terme

ECMWF

Series: ECMWF ESA Project Report Series

A full list of ECMWF Publications can be found on our web site under:
http://www.ecmwf.int/publications/

Contact: library@ecmwf.int

European Centre for Medium Range Weather Forecasts
Shinfield Park, Reading, RG2 9AX, England

Contract Report to the European Space Agency

Support-to-Science-Element (STSE) Study EarthCARE Assimilation

WP-3100 report: Data monitoring experiments for radar and lidar

Authors: S. Di Michele and M. Janisková

ESA ESTEC contract 4000102816/11/NL/CT

August 2013, updated February 2014

ABSTRACT

The feasibility of detecting possible problems with CloudSat and CALIPSO data has been investigated by monitoring statistics over a three-month period. Radar and lidar instrument anomalies increasing in time have been simulated in the measurements. A basic alert system based on threshold levels has been devised to test if these anomalies could be then identified thorough monitoring. Time series of CloudSat reflectivity and CALIPSO cloud backscatter have been generated using the original and degraded observations. The temporal evolution of their corresponding first-guess departures has been also evaluated to investigate if the problems would be identified earlier in the time series.

Results show that the drift in CloudSat and CALIOP observations can be revealed by their time-monitoring. However, performing the monitoring of the first-guess departures resulted in an earlier detection only for CloudSat, while the current discrepancies between CALIOP observation and simulated cloud backscatter are preventing a similar gain.

Contents

1 Introduction

At the European Centre for Medium Range Weather Forecasts (ECMWF), every new observation before being actively assimilated in the operational analysis system is first monitored for a period of time. In order to check that the requirements for assimilation are met, model-vs-observation statistics are evaluated in time using the Numerical Weather Prediction (NWP) model as a reference point. This process also constitutes a unique tool to routinely check the data quality by comparison with the corresponding model first-guess (FG). Not only operational satellites, but also the research ones can benefit from the monitoring activity. The European Space Agency (ESA) is preparing the Earth, Clouds, Aerosols and Radiation Explorer (EarthCARE) research satellite, planned for launch in 2016, which will use a combination of a lidar (ATLID) and a cloud radar (CPR) to provide the vertical structure and the horizontal distribution of cloud and aerosol over all climate zones. Currently available space-borne lidar and radar observations from the CloudSat (Stephens et al., 2002) and CALIPSO (Winker et al., 2009) provide a source of data to be used for feasibility studies in preparation for the future EarthCARE mission. A number of studies (Janisková, 2004; Lopez et al., 2006; Janisková et al., 2012) have shown that, when assimilated into NWP models, these observations have the potential to improve their initial atmospheric state.

This report summarizes the results of the work done under Work Package 3100 of the ESA-funded Support-to-Science Element (STSE) study on EarthCARE assimilation. Closely resembling the approach followed in Di Michele et al. (2014b,a), monitoring experiments are performed using data from the CloudSat radar and the CALIOP (Cloud-Aerosol Lidar with Orthogonal Polarization) lidar on board CALIPSO. In particular, monitoring tests have been performed in order to understand the skill that the monitoring system has in detecting a potential degradation in the quality of observations. First, Section 2 considers the monitoring of CloudSat data, both in terms of reflectivities and cloud-top height derived from reflectivity observations. Then, in a similar way, the results of lidar monitoring experiments are described in Section 3. Conclusions from the monitoring experiments on both instruments are finally provided in Section 4.

2 CloudSat radar monitoring

Monitoring of CloudSat data together with the ECMWF model equivalents have been performed, first concentrating on temporal evolution of the radar reflectivity from CloudSat observations (Subsection 2.1) and then taking into account cloud top height as derived from the reflectivity (Subsection 2.2).

2.1 Monitoring of radar reflectivity

Time series of CloudSat stand-alone observations and FG departures are considered for monitoring, similarly to Di Michele et al. (2014b). Reflectivity FG departures have been evaluated running the ZmVar radar operator (Di Michele et al., 2012) on the atmospheric profiles extracted from the ECMWF short-term forecasts. The performed studies in Di Michele et al. (2014d) and Di Michele et al. (2014b) clearly showed that the forecast model is able to realistically reproduce the cloud structures, capturing all main features. Larger discrepancies were observed in the tropical regions since these tropical cloud regimes are the most difficult to represent given their small scale and short temporal duration that can lead to errors in intensity and/or location (see Fig. 2.1 and Fig. 2.2 for illustration). Given a good agreement between observations and the model equivalent, the experiments have been done to investigate whether data quality monitoring can benefit from using the FG departures compared to the monitoring of observations alone.

2.1.1 Time series of reflectivity

The radar reflectivity factor Z (or simply reflectivity) at a given wavelength (λ) is defined as:

$$Z = \frac{\lambda^4}{\pi^5 |K_w|^2} \eta \tag{2.1}$$

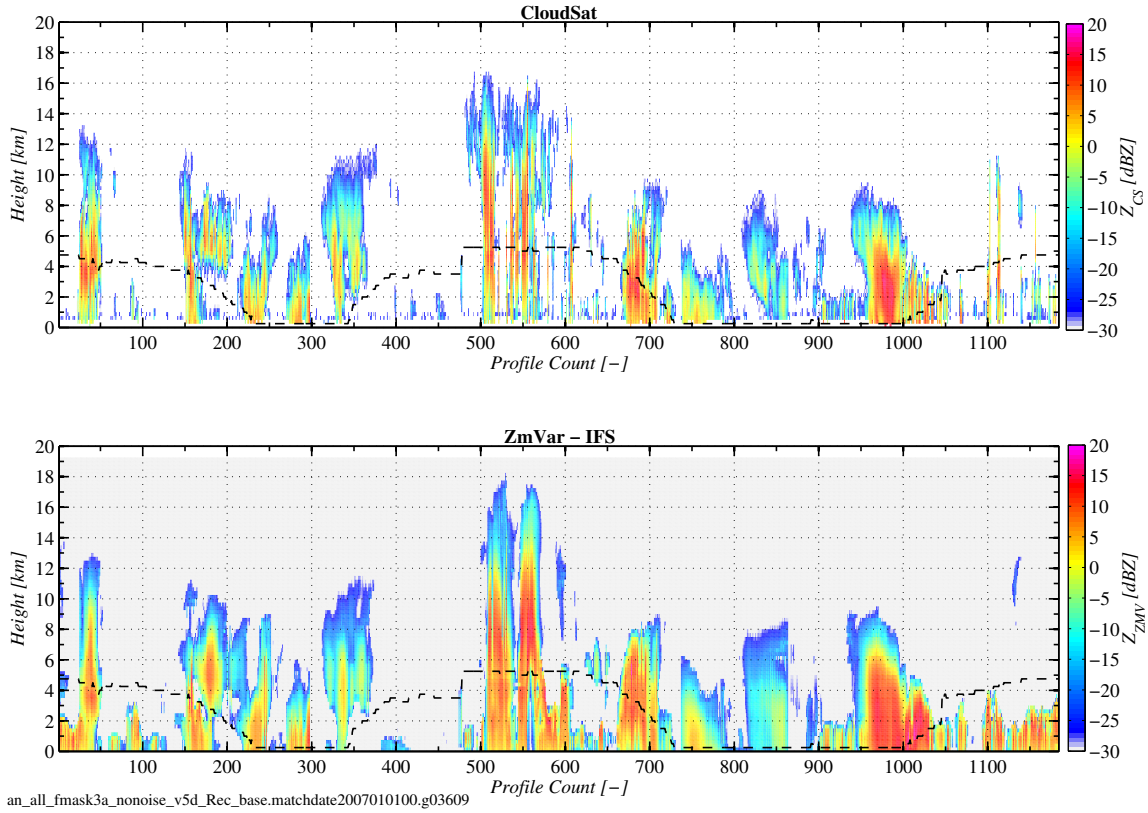

Figure 2.1: Top panel: CloudSat observations (averaged to model resolution) along granule 3609 on 1 January 2007. Bottom panel: the corresponding simulated reflectivities using ZmVar on the ECMWF model short-term forecasts.

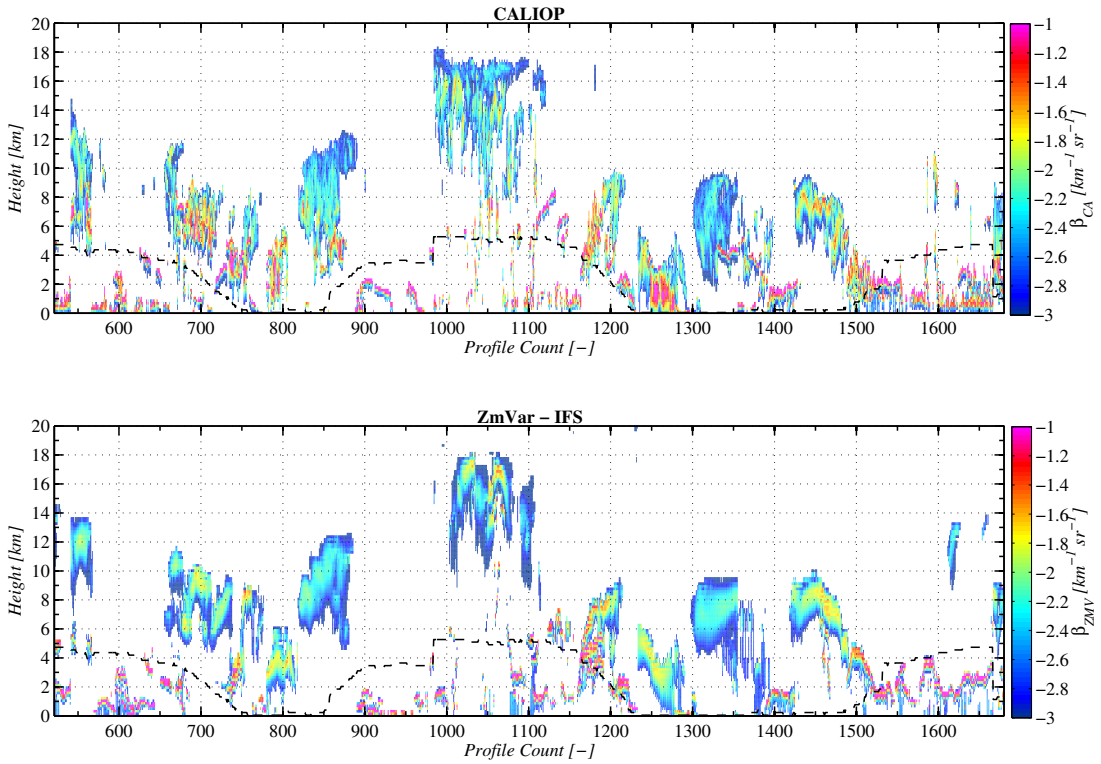

Figure 2.2: Top panel: Cloud backscatter (averaged to model resolution) observed by CALIOP on 1 January 2007. Bottom panel: corresponding values simulated by ZmVar using the ECMWF model short-term forecasts.

where η is the volumetric backscatter cross section due to the target and K_w is the dielectric factor of liquid water at 10°C (and wavelength λ). η is related to the received power P_r through the radar equation:

$$\eta = C\frac{P_r}{P_t}r^2 \tag{2.2}$$

where r is the target distance to the radar, P_t is the power radiated by the radar and C is the radar constant, which takes into account the instrument design characteristics (e.g. the antenna gain and radar pulse integral). The correct definition of the radar constant (i.e. a good calibration) is crucial for the quality of measurements.

In order to understand if monitoring FG departures has some advantages compared to reflectivity alone in identifying glitches in the instrument, an experiment with degraded quality of CloudSat data has been performed. Considering the period from 1 December 2006 to 28 February 2007 for the study, an instrument degradation has been mimicked by drifting away a radar constant starting from the beginning of January 2007 until the end of February (i.e. the end of three month period). If the value C_b specified for the calibration constant is different from the real one C by a factor K_b, this gives rise to a bias in reflectivities expressed in dBZ (Z_{dB}):

$$C_b = K_b C \Longrightarrow Z_b = K_b \cdot Z \Longrightarrow Z_b^{dB} = Z^{dB} + 10 \cdot log_{10}(K_b) \tag{2.3}$$

In this experiment, we assume a 1% decrease in C_b every day, leading to a bias of 3 dBZ after two months (i.e. the end of three month period).

Monitoring of stand-alone observations

Figures 2.3 and 2.4 show, for Southern mid-latitudes (30°S-60°S) and tropics (30°S-30°N) respectively, the temporal evolution of the (daily) mean CloudSat reflectivity $\overline{Z_{CS}}$ over the selected three-month period. Radar reflectivity is monitored at five reference heights ranging from 2 km to 10 km, every 2 km. In each plot, dashed lines refer to the monitoring of the untouched observations (reference), while solid lines indicate the experiment where a bias has been added. In addition, blue dots indicates statistical significance of the daily statistics: values of mean and standard deviation are supposed to be robust when at least 100 samples are used for their evaluation. The horizontal dashed lines define the limits for the ordinary range of variation of $\overline{Z_{CS}}$: red lines indicates 110% of the maximum and minimum values, while black lines are for the 90%. The use of two sets of limits allows the definition of two grades of warning, reducing the risk of false alarm. For convenience, in this study the range of variation is evaluated based on the reference run of the monitoring (over the same three months), considering only the occurrences flagged as statistical significant. However, the best values to be used in a real-time monitoring system should be subject of a specific investigation.

The alert messages, that a warning system applied to the time series of the biased $\overline{Z_{CS}}$ would issue, are also indicated in the plots. Black and red circles indicate when the upper and higher limits are exceeded, which would trigger a warning message. Occurrences when the high-warning (red) occurs consecutively in more than one instance are marked with a star symbol. A more severe message (alarm) should correspond to these situations, since the higher limit is exceeded more than once.

In our experiment, when considering mid-latitudes (Fig. 2.3), we note that no alarm messages are issued, but only few sparse warnings. On the contrary, in the tropics (Fig. 2.4), the first alarm (red asterisk) occurs for $\overline{Z_{CS}}$ at 2 km on 8 February 2007, repeating in the following days. This better skill in identifying the problem is due to the lower range of variation of $\overline{Z_{CS}}$ in the tropics compared to the same quantity at mid-latitudes.

The standard deviation of observations is the second quantity usually employed in a monitoring system beside the mean. Figures 2.5 and 2.6 show the standard deviation of CloudSat reflectivity $\sigma_{Z_{CS}}$. Interestingly, in all plots we notice that the negative bias results in a negative trend also for the standard deviation. This is a consequence of the presence of a cut-off value for observations (the minimum detectable signal) due to which the negative bias in observations leads to a reduction of the dispersion. For the same reason as for the mean, we notice that the effect of the bias trend is more pronounced at the levels with larger signal, i.e. 2 km and 4 km. For $\sigma_{Z_{CS}}$ at mid-latitudes (Fig. 2.5), both the first high-warning and the first alarm occur at 2 km, on

21 January 2007 and on 7 February 2007, respectively. Therefore, comparing $\sigma_{Z_{CS}}$ with $\overline{Z_{CS}}$ at mid-latitudes, we notice that the former is more efficient in detecting the bias. The same result is found in the tropics. Figure 2.6 shows that the first alarm is triggered by $\sigma_{Z_{CS}}$ (at 4 km) on 27 January 2007, ten days earlier than by $\overline{Z_{CS}}$ monitoring.

Monitoring of FG departures

The monitoring of CloudSat FG departures follows the same approach used for stand-alone observations, but using only the data satisfying the screening conditions described in Di Michele et al. (2014d) (Subsection 4.1). Figures 2.7 and 2.8 show the time series of the daily mean reflectivity departures $\overline{\delta Z}$ separately for mid-latitudes and tropics. In both cases, as seen for $\overline{Z_{CS}}$, we notice that the negative trend of the biased $\overline{\delta Z}$ becomes more and more evident moving toward lower altitudes. At mid-latitudes (top panel in Fig. 2.7), the results at 10 km should not be considered because of the lack of meaningful statistics (since only one day has at least 100 cases). Therefore no warning or alarm are issued though the defined limits are clearly exceeded there. When considering the altitudes below, the first warning and alarm messages occur at 2 km, respectively on 19 January 2007 and 3 February 2007. We can notice that the effect of the bias on the $\overline{\delta Z}$ temporal evolution is most evident at this level: alarms are continuously repeated from the first occurrence. When comparing with the performance of $\overline{Z_{CS}}$ at mid-latitudes, where no alarm was triggered, we clearly see the advantage of using FG departures. Evaluation of the results in the tropics (Fig. 2.8) is not possible because of the poor number of observations retained after screening. However, we notice that the first alarm appears at 8 km on 28 January 2007and the second one at 2 km on 8 February 2007, corresponding (by date and level) to the first alarm occurred by monitoring of $\overline{Z_{CS}}$.

The temporal evolution of standard deviations of CloudSat FG departures $\sigma_{\delta Z}$ at mid- latitudes and tropics is shown in Fig. 2.9 and Fig. 2.10, respectively. At mid-latitudes (Fig. 2.9), after disregarding the results at 10 km for the same reasons as mentioned above, we note that the first high-warning, appears (at 2 km) already on 7 January 2007, but the second (again at 2 km) occurs only on 25 January 2007 and an alarm is triggered on 15 February 2007. Overall, the picture shows that at mid-latitudes there is not a clear advantage of $\sigma_{\delta Z}$ over $\sigma_{Z_{CS}}$. The analysis of $\sigma_{\delta Z}$ in the tropics (Fig. 2.10) is as before hampered by availibility of only few days when the number of cases over one day, n_{CS}, is larger than 100. Despite of this, the plots shows that the alarm is triggered few times. The comparison with $\sigma_{Z_{CS}}$ in 2.6 shows a similar timing of alarms.

Monitoring number of observations passing the screening

The number of observations passing the screening also constitutes an important piece of information for monitoring. It complements the departures since a drop in their number would indicate a decrease in agreement (because of less cases passing through the screening). Figures 2.11 and 2.12 show the temporal series over three months (December 2006 to February 2007) of the number of CloudSat observations (averaged to the model grid box) at Southern mid-latitudes ($30°S$-$60°S$) and in the tropics ($30°S$-$30°N$), respectively. For selected altitudes, each plot contains (in different colors) the number of observations before and after the screening falling into either a 12-hour or 24-hour window. Both at mid-latitudes and tropics, roughly one third of the data are retained. However, at mid-latitudes above 10 km, most of the data are rejected by the screening because of the poor correlation between observations and simulations. In absolute terms, after screening at mid-latitudes there are about 200 observations per day, while in the tropics they are about 100. The 12-hour observations are (as expected) roughly half of the daily ones, and therefore after screening their sample is too small to compute reliable statistics. For this reason, the monitoring analysis is done considering quantities computed as daily mean. With this window length, the sample size after screening is large enough to be able to evaluate time series. Note that the lack of data on the 16 February 2007 is due to problems in the forecast processing. For all other days, these series are quite stable in time, thus indicating that a problem in model (as in the above mentioned case) or in observations could be detected by monitoring the time series of number of observations over 24-hour window.

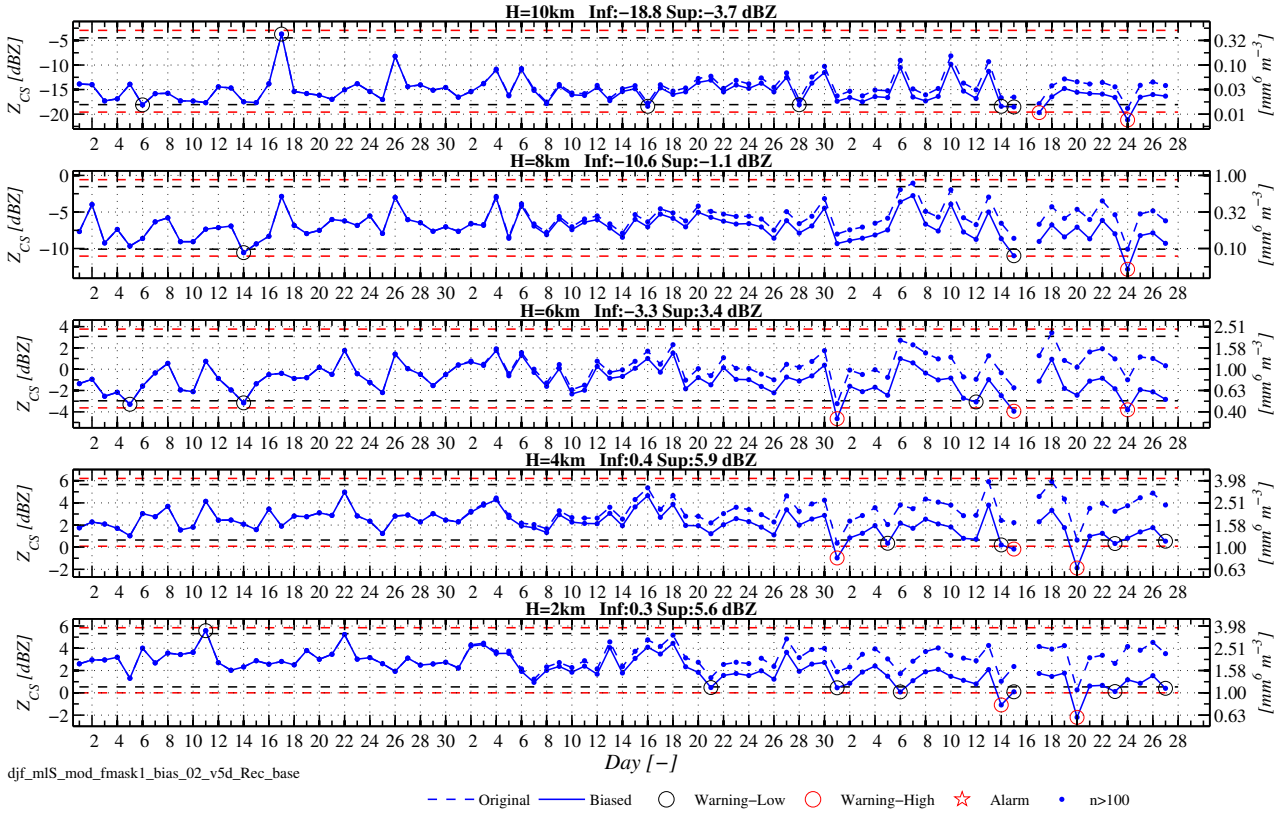

Figure 2.3: Time series of daily mean CloudSat reflectivity for the period from 1 December 2006 to 28 February 2007, considering observations at mid-latitudes South (30°S-60°S). Different panels contains data at the altitude level (H) shown in the title. Blue dashed line is for original observations, while blue solid line with artificial bias added. Horizontal lines define the limits used for warning system. See text for more explanation.

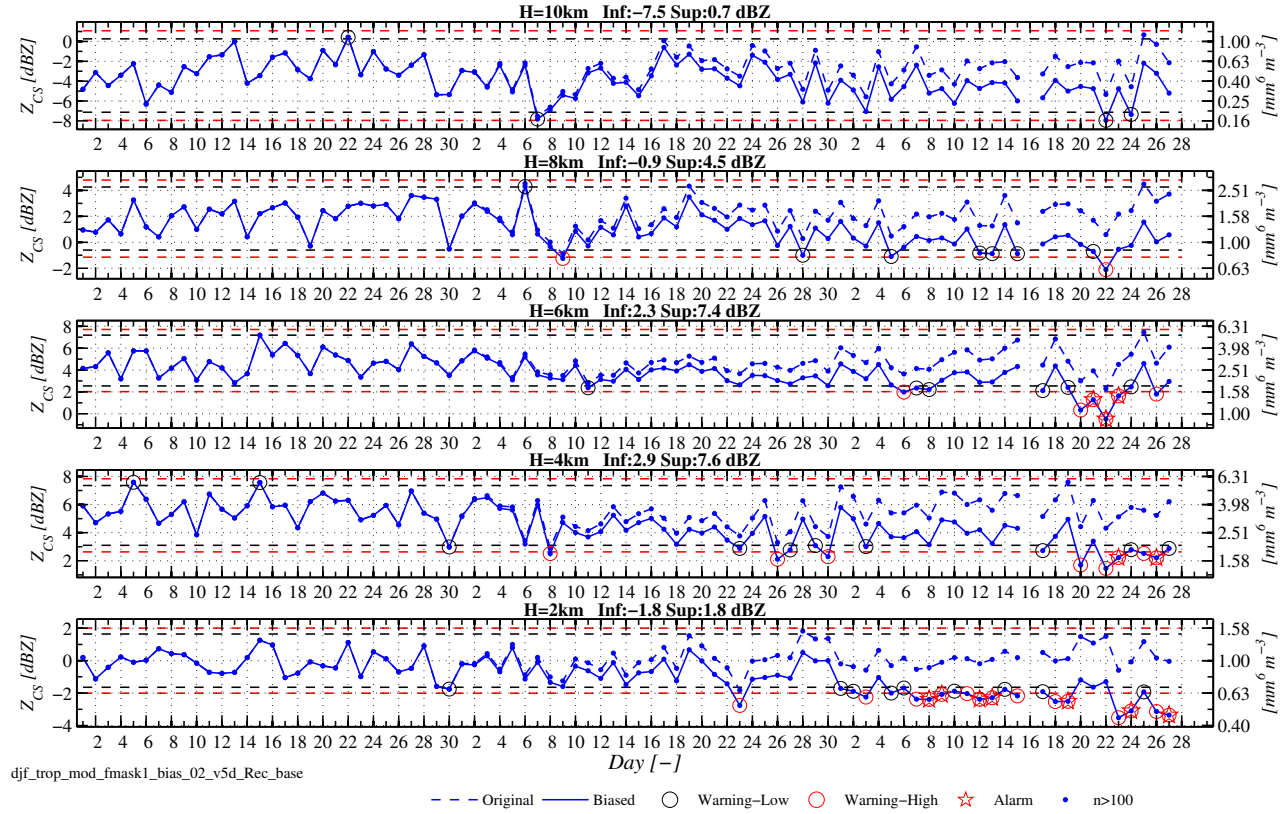

Figure 2.4: Same as 2.3, but considering observations in the tropics (30°S-30°N).

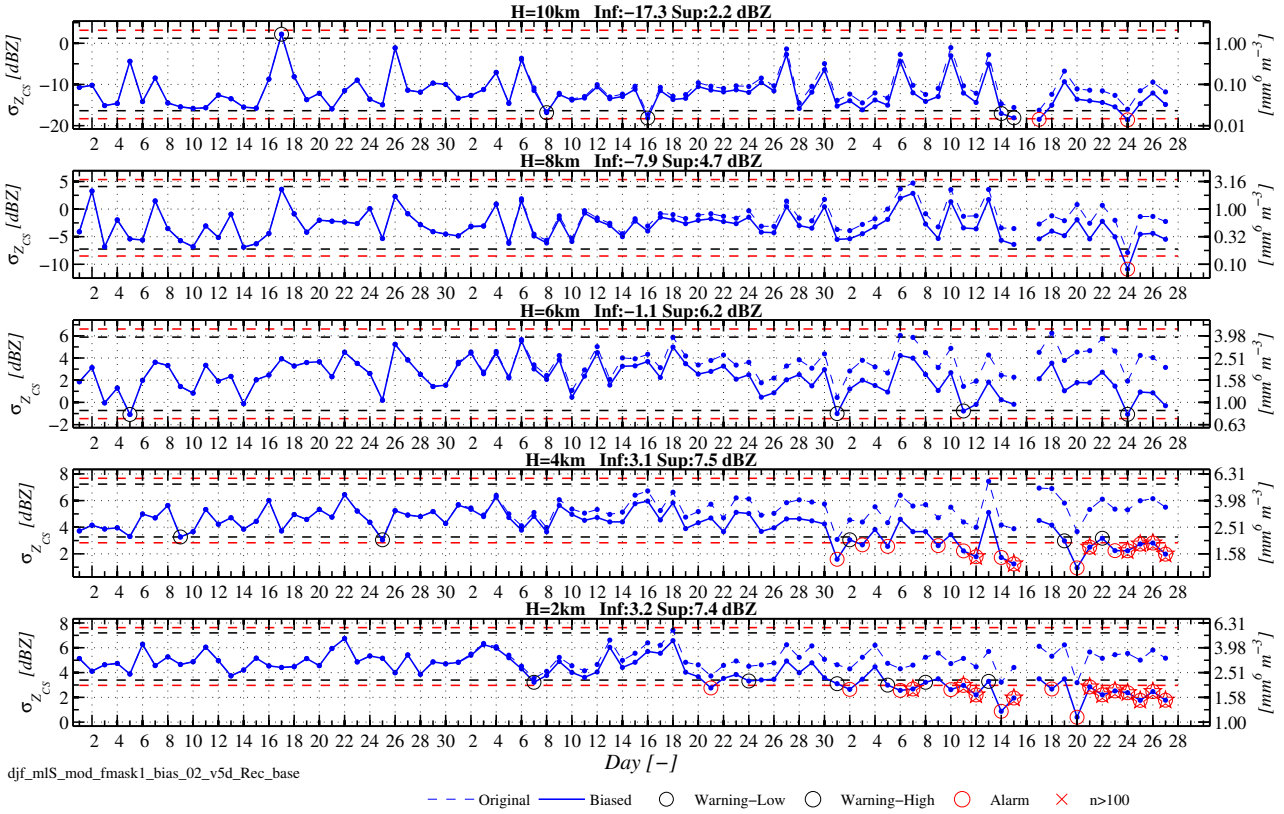

Figure 2.5: Same as 2.3, but for time series of CloudSat reflectivity standard deviation considering observations at mid-latitudes South (30°S-60°S).

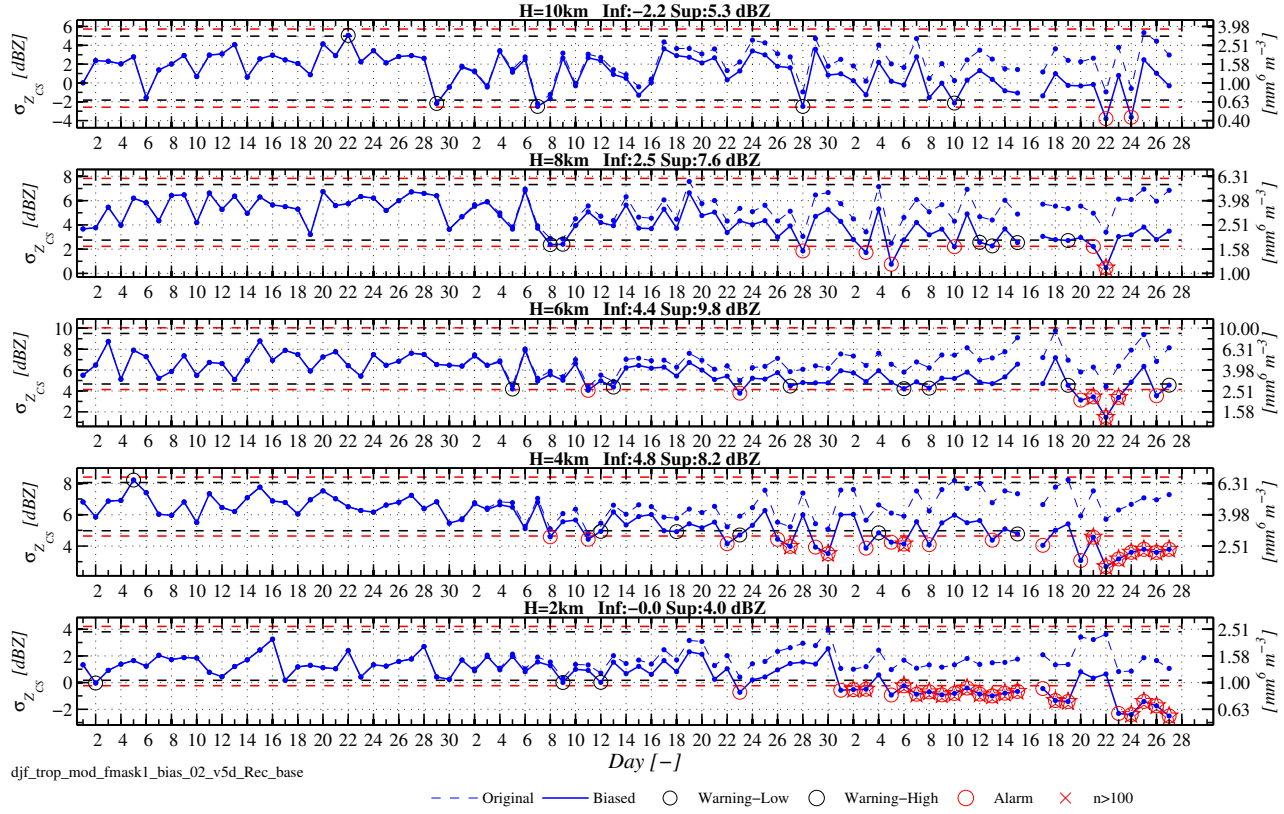

Figure 2.6: Same as 2.5, but considering observations in the tropics (30°S-30°N).

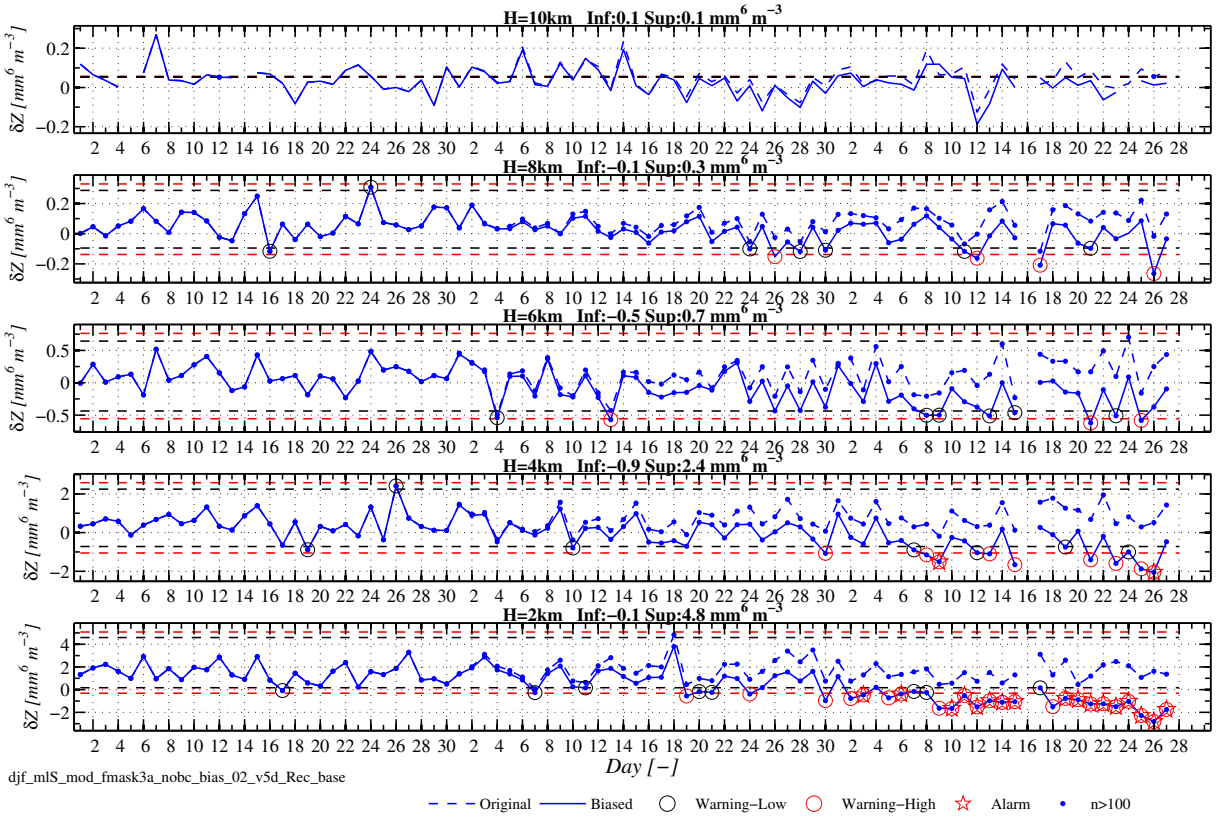

Figure 2.7: Same as 2.3, but for time series of CloudSat mean reflectivity first-guess departures considering observations at mid-latitudes South (30°S-60°S).

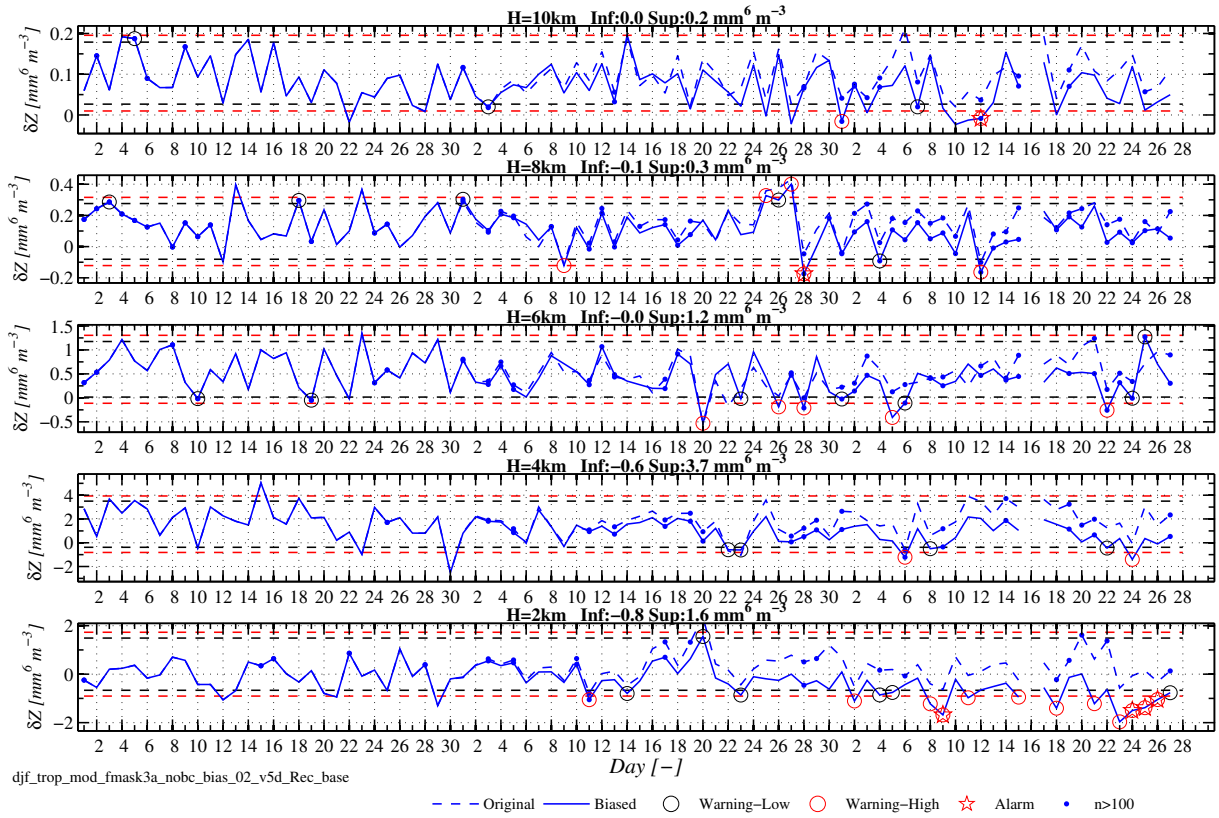

Figure 2.8: Same as 2.7, but considering observations in the tropics (30°S-30°N).

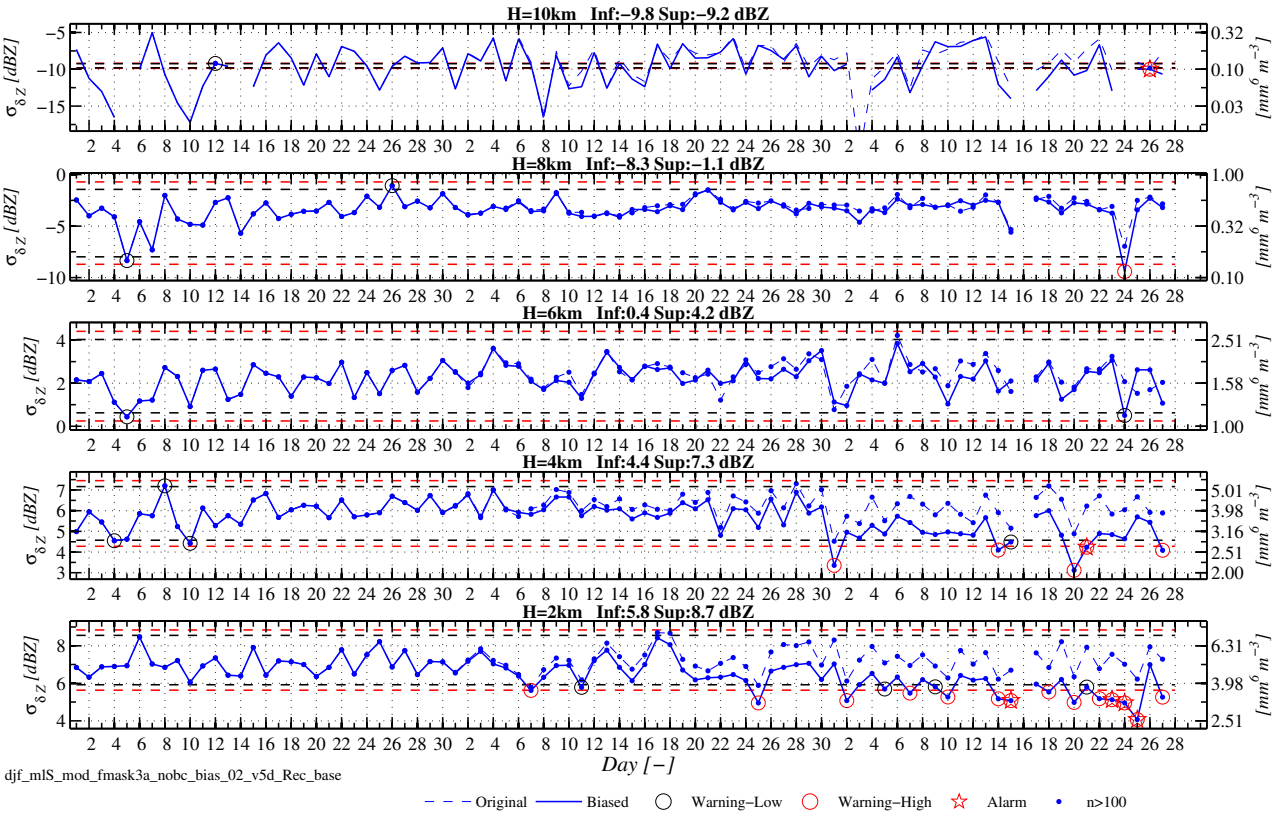

Figure 2.9: Same as 2.3, but for time series of CloudSat reflectivity first-guess departure standard deviation considering observations at mid-latitudes South (30°S-60°S).

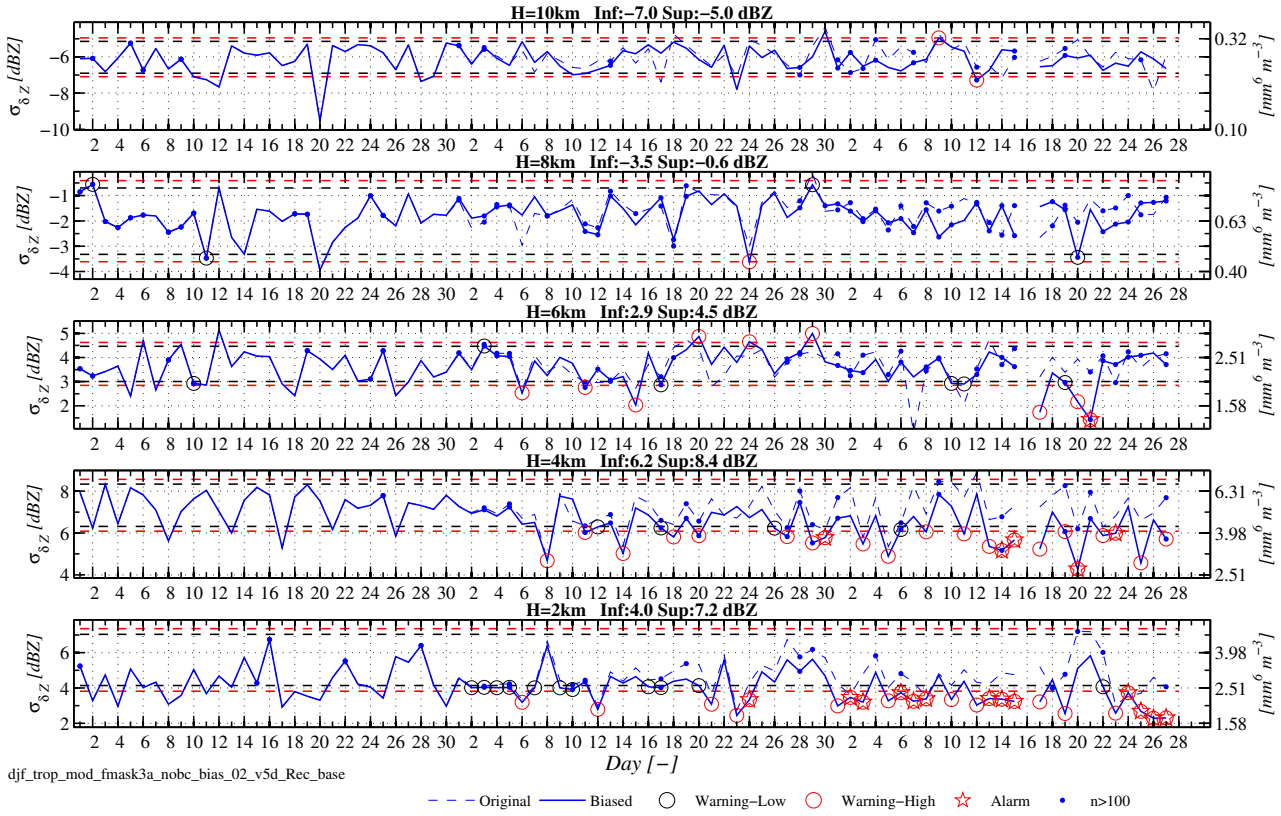

Figure 2.10: Same as 2.9, but considering observations in the tropics (30°S-30°N).

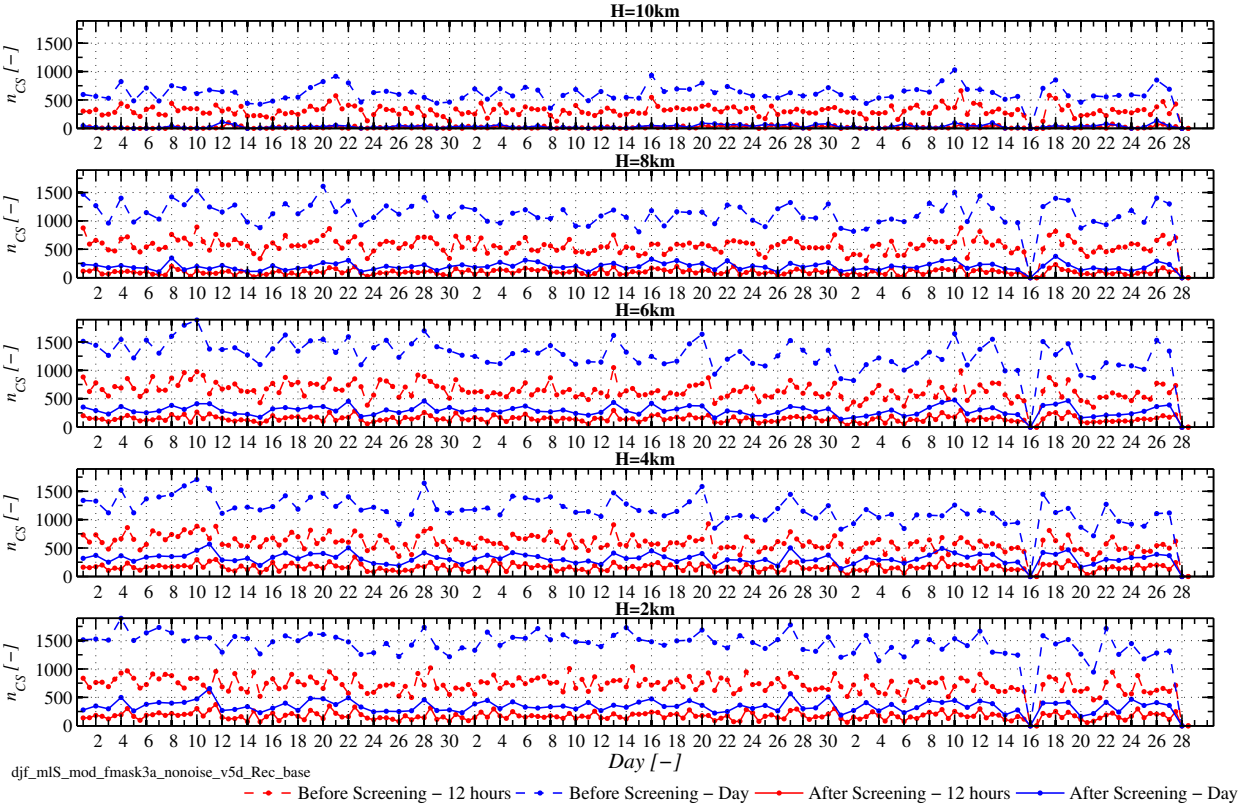

Figure 2.11: Time series of CloudSat reflectivity sample number for the period from 1 December 2006 to 28 February 2007, considering observations at mid-latitudes South (30°S-60°S). Dashed and solid lines indicate data before and after screening, respectively. Red and blue lines refer to 12- and 24- hour time window stepping. Different panels contains data at the altitude level (H) shown in the title.

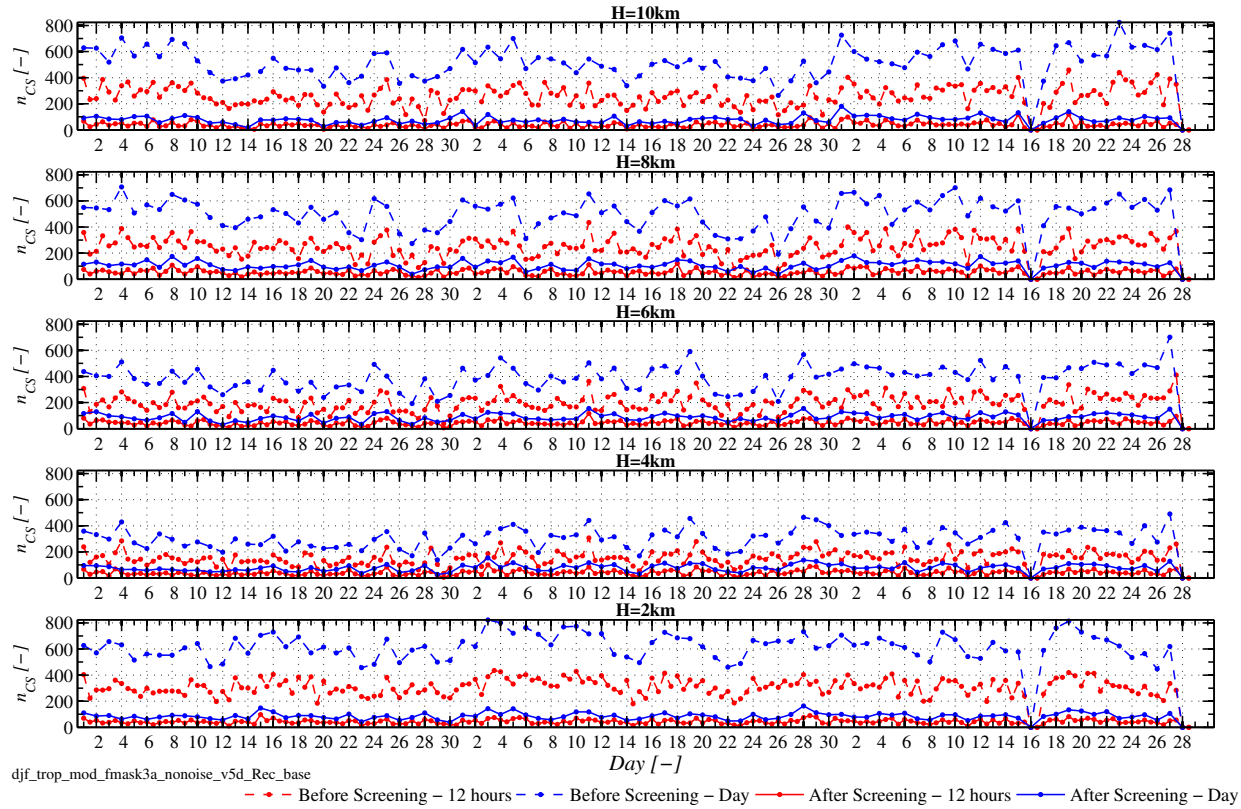

Figure 2.12: Same as 2.11, but considering observations in the tropics (30°S-30°N).

2.2 Monitoring of cloud-top height from radar

In this section, the monitoring of cloud-top height (CTH) derived from CloudSat reflectivity measurements is considrered. The investigation in Di Michele et al. (2014b) demonstrated that this quantity has the potentials to be used for monitoring.

Similarly to the monitoring of reflectivity in Section 2.1, the impact of the same bias drift on the monitoring will be investigated in Subsection 2.2.1, where Cloudsat CTH will be taken into account both as stand-alone variable and as FG departure evaluated from the IFS forecasts. The detection of bias through CTH departures monitoring has been performed considering independently the two screening conditions (clouds below 5 km and clouds above 5 km). In the following, only the monitoring of high clouds will be reported since it is the one that gives the best results, and therefore better representing the CTH monitoring possibilities.

2.2.1 Time series of cloud-top height

Stand-alone CTH

The temporal evolution over the three-month study-period of the daily mean CTH from CloudSat $\overline{h_{CS}^{top}}$ is shown in Fig. 2.13 separately for Southern mid-latitudes (30°S-60°S) and tropics (30°S-30°N). In each plot, lines and symbols have the same meaning used in the reflectivity monitoring. In principle, given the bi-modal distribution of CTH, the analysis for situations below or above 5 km should be done separately. Here, for consistency for the used screening, only CTH values above 5 km are considered. For this reason, $\overline{h_{CS}^{top}}$ is between 9 and 10 km at mid-latitudes (top panel) and between 11 and 12 km in the tropics (bottom panel).

The main feature of these plots is that the negative bias induced into CloudSat observations translates into a decreasing trend for the CTH that is not large enough to trigger an alarm. Figure 2.14 shows that the same behaviour can be observed for the monitoring of the standard deviation ($\sigma_{h_{CS}^{top}}$).

CTH departures

The results from the experiments considering CTH departures, $\overline{\delta h^{top}}$, as monitoring quantity are shown in Fig. 2.15. At mid-latitudes (top panel), the first alarm (red asterisk) occurs only on 27 February 2007, while the first warning (red circle) happens one month before, repeating for three times. In the tropics (bottom panel), only warnings are issued, the first one on 6 February 2007. The comparison with Fig. 2.13 shows that the monitoring of $\overline{\delta h^{top}}$ is able to provide better indications about the drifting, mainly because of its smaller range of variation. However, due to the day-by-day oscillations of the time series, the warnings translate into an alarm only very late. As shown in Fig. 2.16, the standard deviation of CTH departures $\sigma_{\overline{\delta h^{top}}}$ does not show any clear trend that would point to a drift in the observations.

Number of CTH cases

Figure 2.17 shows the time series of the number of CTH cases, $n_{h^{top}}$, over three months (December 2006 to February 2007) at Southern mid-latitudes (30°S-60°S) and in the tropics (30°S-30°N). In order to display the amount of data retained, each plot contains the number of CTH cases before and after the screening. We notice that, both at mid-latitudes and tropics, roughly half of the data pass through the screening. The plots shows (in different colors) $n_{h^{top}}$ over 12-hour and a 24-hour. However, similarly as for the reflectivity monitoring, the daily statistics should only be considrered since they provide a more reliable sample.

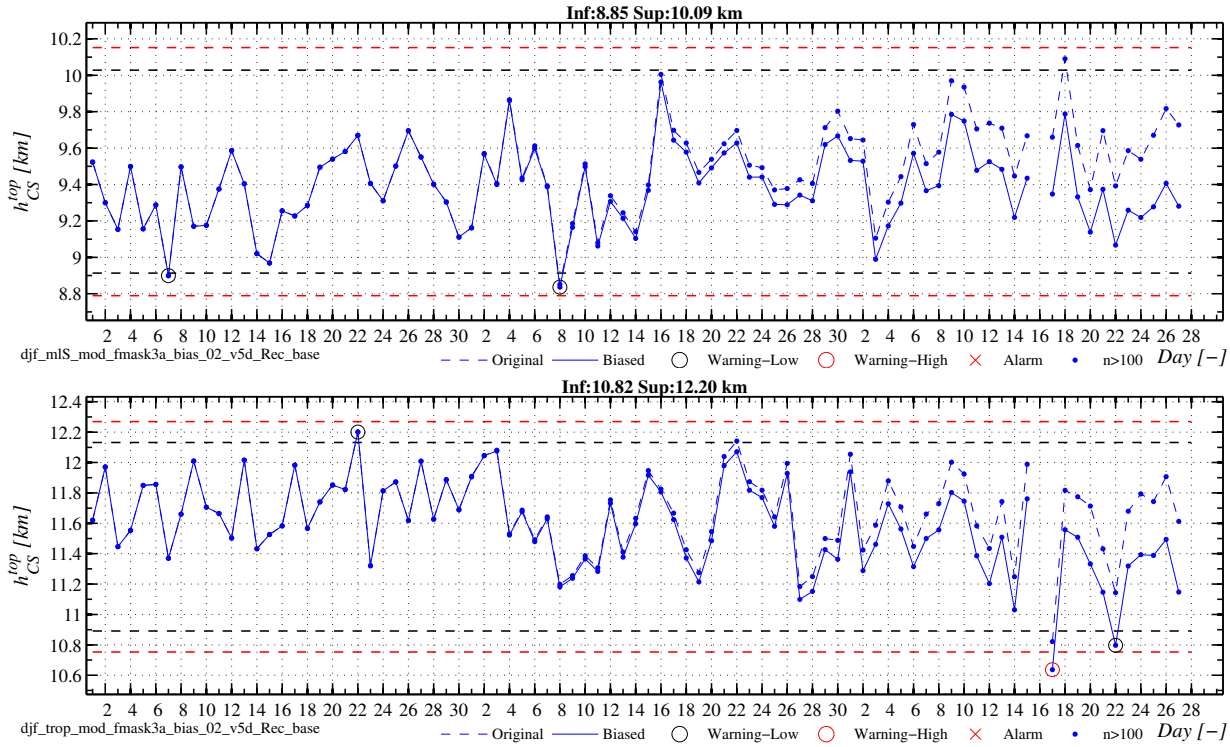

Figure 2.13: Time series of mean CloudSat-derived CTH for the period from 1 December 2006 to 28 February 2007. Blue dashed line is for original observations, while blue solid line with artificial bias added. Top panel is for observations at mid-latitudes South (30°S-60°S), and bottom panel uses observations in the tropics (30°S-30°N).

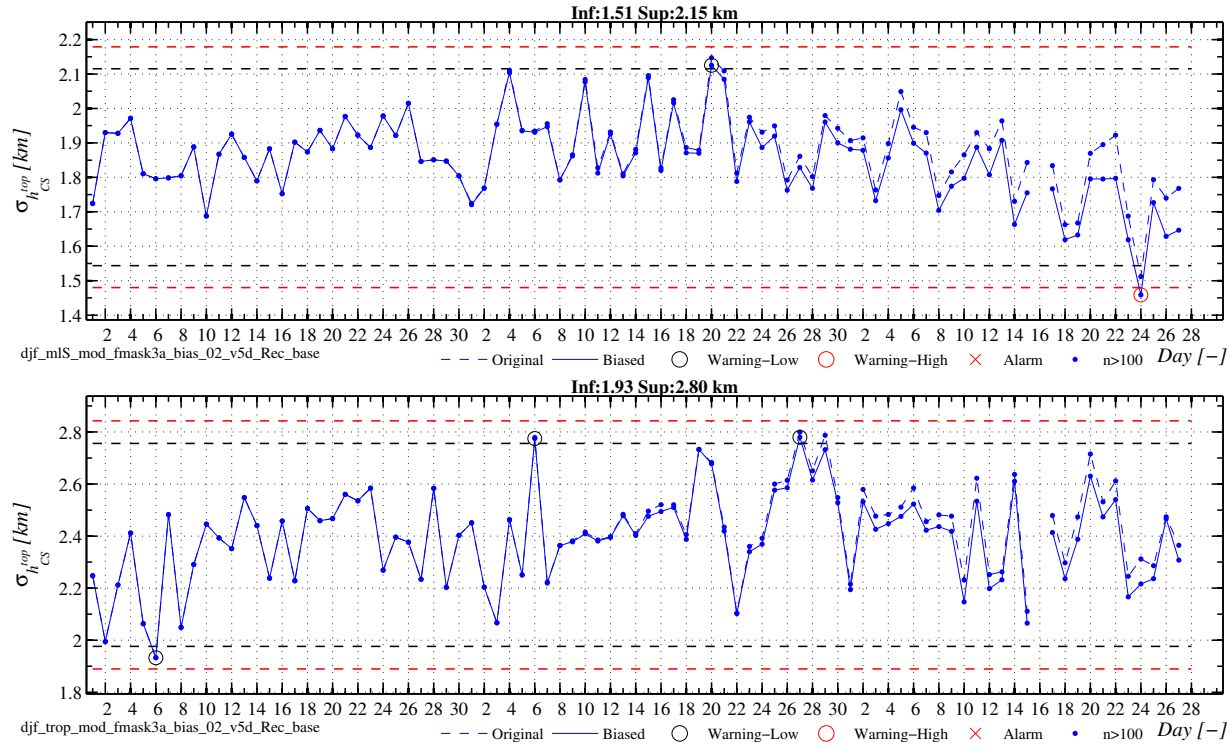

Figure 2.14: Same as 2.13, but for standard deviation time series of CloudSat-derived cloud-top height.

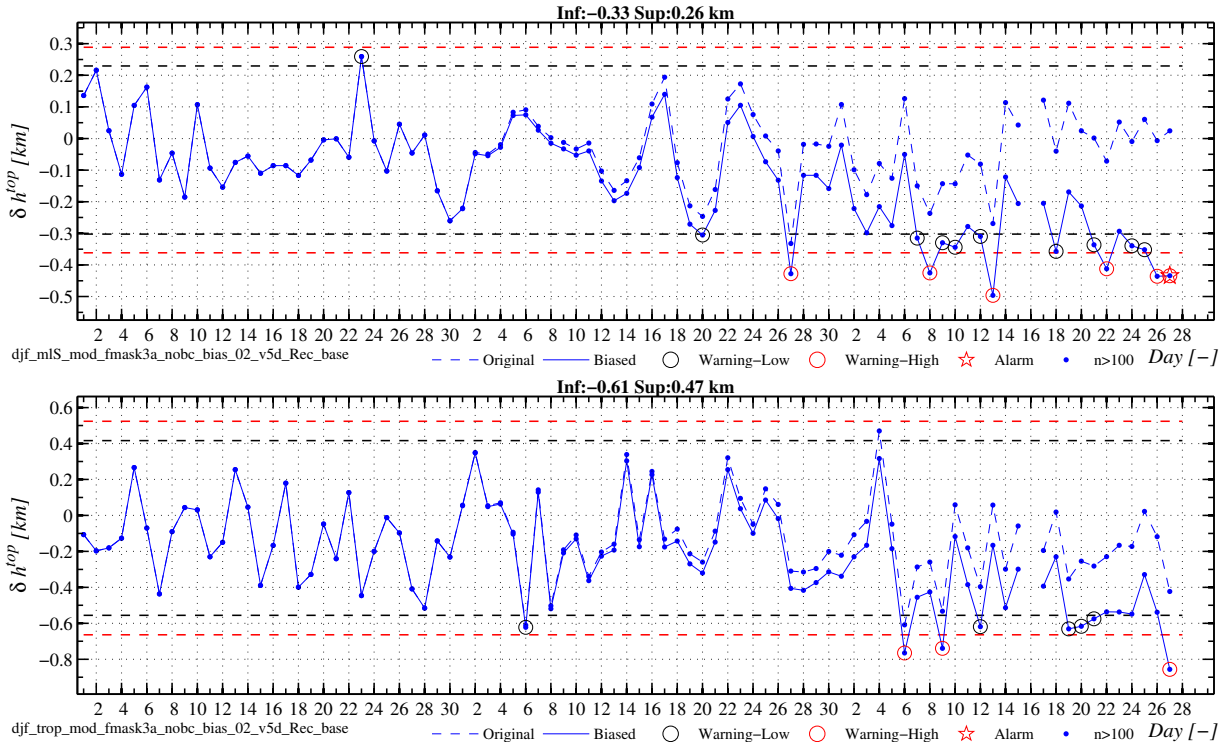

Figure 2.15: Same as 2.13, but for time series of mean differences between CloudSat-derived cloud-top height and ZmVar-IFS equivalents.

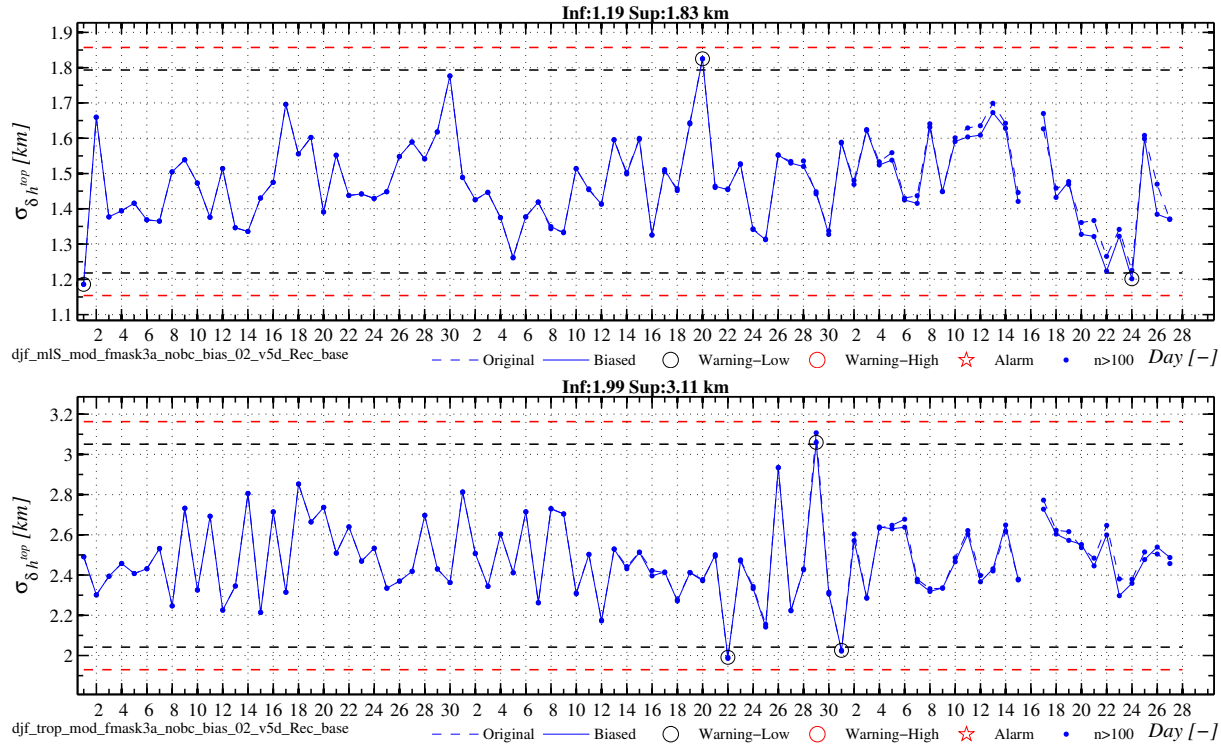

Figure 2.16: Same as 2.13, but for time series of standard deviation of differences between CloudSat-derived cloud-top height and ZmVar-IFS equivalents.

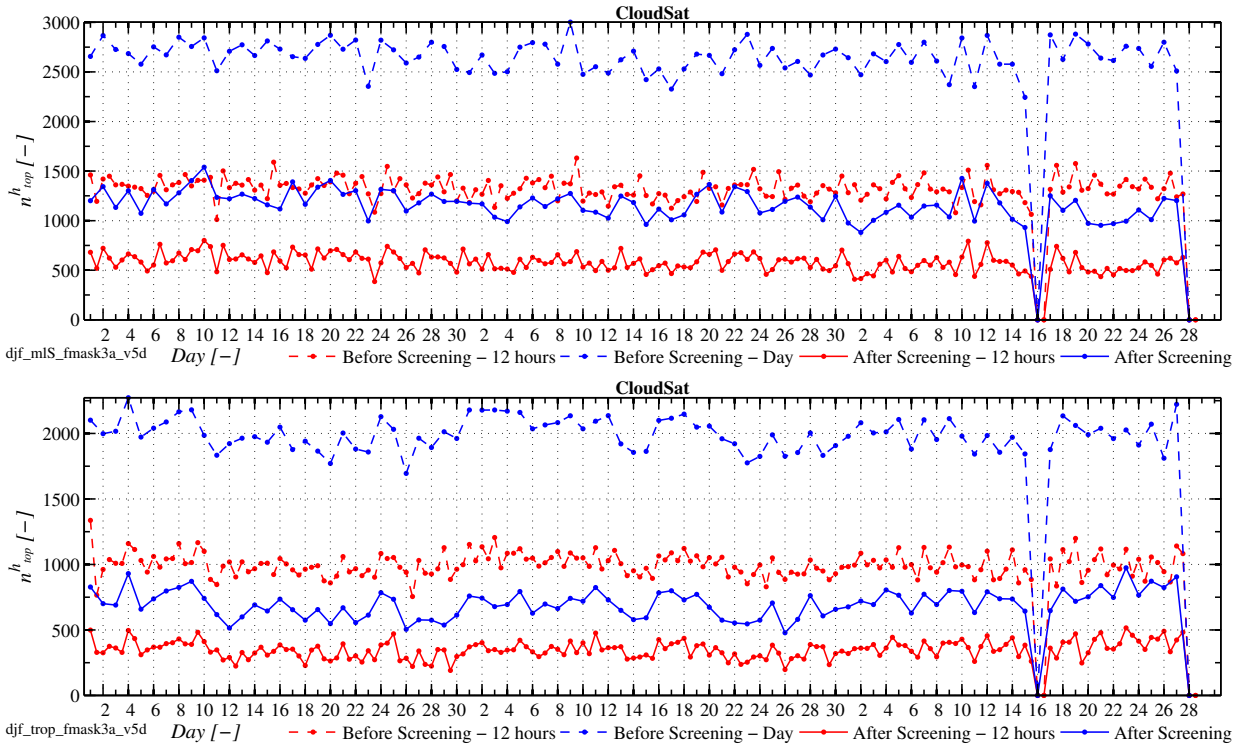

Figure 2.17: Time series of sample number of cloud-top height from CloudSat for the period from 1 December 2006 to 28 February 2007. Dashed and solid lines indicate data before and after screening. Red and blue lines refer to 12- and 24- hour time window stepping, respectively. Top panel is for observations at mid-latitudes South (30°S-60°S), and bottom panel uses observations in the tropics (30°S-30°N).

3 CALIPSO lidar monitoring

Monitoring cloud-related data obtained from the CALIOP lidar onboard CALIPSO has been also investigated. Monitoring experiments have been performed with the purpose of understanding if there are any advantages in the use of a forecast model for the purpose of data quality analysis. As done for CloudSat in Section 2, two distinct quantities are used as monitoring variables. In Subsection 3.1 the lidar backscatter due to clouds is considered, while the derived height of cloud top is taken into account in Subsection 3.2.

3.1 Monitoring of cloud backscatter

As done for CloudSat observations, an strategy for monitoring cloud backscatter in the context of an assimilation system will be investigated. In principle, if observations are accurately simulated by the NWP forecast model, a continuous monitoring of their differences would provide a better identification of problems in the data than it would be produced using observations only.

3.1.1 Time series of cloud backscatter

In order to understand if the monitoring of backscatter FG departures has some advantages in identifying glitches in the instrument, experiments have been performed where the quality of CALIOP data has been degraded. The lidar backscatter β can be written as function of the instrument variable as:

$$\beta = C\frac{S}{E_0 G_A}r^2 \tag{3.1}$$

where r is the distance to the lidar, S is the measured signal after subtraction of solar background and digitizer offset voltages, E_0 is the laser energy, G_A is the amplifier gain, and C is the lidar calibration coefficient. As done for CloudSat, using the period from 1 December 2006 to 28 February 2007 for the monitoring, a drift in the value of the lidar calibration coefficient C has been imposed, decreasing 1% every day from 1 January 2007.

Monitoring of stand-alone observations

Using the same symbol convention used in Section 2, Fig. 3.1 and Fig. 3.2 show the monitoring of the mean CALIOP cloud backscatter $\overline{\beta_{CA}}$ over the considered period under consideration, for Southern mid-latitudes ($30^\circ S$-$60^\circ S$) and tropics ($30^\circ S$-$30^\circ N$) respectively. Cloud backscatter is monitored at five different heights, from 4 km to 12 km, every 2 km. When considering the mid-latitude case (Fig. 3.1), a more pronounced drift can be noticed at higher altitudes, where the backscatter usually reaches larger values. The first alarm (on 11 February 2007) occurs at 8 km because at this altitude the backscatter exhibits a range of variation smaller than at other levels.

In the tropics (Fig. 3.2), a clear effect of the drift in C can be seen above 10 km. In particular, the backscatter monitoring is the most capable of identifying the drift at 12 km. In fact, at this altitude time fluctuations are small and backscatter values quite high, allowing the first alarm to be triggered already on 21 January 2007. On the contrary, the same figure shows that a reliable monitoring is not possible at altitudes below 8 km mainly because of the lack of samples.

The corresponding time series of (daily) CALIOP backscatter standard deviations $\sigma_{\beta_{CA}}$ are shown in Fig. 3.3 and Fig. 3.4, for Southern mid-latitudes and tropics respectively. As seen for reflectivity and for the same reason, the continuous decrease of the lidar calibration coefficient also causes a decrease in $\sigma_{\beta_{CA}}$. In the lidar case, the molecular backscatter derived by the model is used as cut-off value for observations, i.e. only the values of (observed or simulated) cloud backscatter above this threshold are taken into account. At mid-latitudes

(Fig. 3.3), the negative trend gives rise to the first alarm at 2 km on 10 February 2007. Consistently with the monitoring of $\overline{\beta_{CA}}$, the drift is well detected also at 8 km, where few warnings are issued at around the same day and the alarm is occurring only 2 days later. In the tropics (Fig. 3.4), again as for $\overline{\beta_{CA}}$, the better detectability is seen at 12 km, where the alarm is triggered on 6 February 2007.

Monitoring of FG departures

Time series of the mean cloud backscatter departures $\overline{\delta\beta}$ are shown in Fig. 3.5 and Fig. 3.6, separately for mid-latitudes and tropics. Statistics are built considering only those cases passing the screening criteria mentioned in Di Michele et al. (2014c) (Section 4.1).

At mid-latitudes (Fig. 3.5), the effect of the $'bias'$ in the CALIOP backscatter is most evident at 8 km and 10 km. Below and above this altitude range, the analysis is compromised by the low number of samples. The comparison with the corresponding time series of daily mean observations of cloud backscatter $\overline{\beta_{CA}}$ (Fig. 3.1) shows that there is not an advantage in the FG monitoring despite $\overline{\delta\beta}$ having a smaller range of variation. Similar conclusions can be drawn for the monitoring of FG departures of CALIOP backscatter in the tropics (Fig. 3.6).

The temporal evolution of standard deviations of CALIOP cloud backscatter FG departures $\sigma_{\delta\beta}$ is shown in Fig. 3.7 and Fig. 3.8, for mid-latitudes and tropics respectively.

Monitoring number of observations passing the screening

Based on the results presented in Di Michele et al. (2014c) (Section 4.1), a simple screening has been set up to retain only the cases with a sufficient good agreement between the modelled and observed backscatter, excluding the cases when differences are larger than $2 \cdot 10^{-3} km^{-1} sr^{-1}$ if above 8 km and larger than $3 \cdot 10^{-3} km^{-1} sr^{-1}$ below 8 km and only considering observations at levels above 4 km. The effect of this screening on the number of monitored observations is shown in Fig. 3.9 and Fig. 3.10, for Southern mid-latitudes ($30^{\circ}S$-$60^{\circ}S$) and tropics ($30^{\circ}S$-$30^{\circ}N$) separately. Each plot contains, over a three month period (December 2006 to February 2007), the temporal series of the number of CALIOP observations n_{CA} at selected altitudes (after averaging to the model grid box). The values that n_{CA} assumes before and after the screening are given as dashed and solid lines, considering both a 12-hour window and a 24-hour one (single day). In December, we note a long period when data are missing. Reason for this is in CALIOP being down until 19 December 2006 because of a solar proton event started on 5 December 2006. The second period of data outage appears between 15 and 17 January 2007 and when the payload was down because the CALIPSO satellite performed a drag make-up maneuver. The data drops on 27 January 2007 and 3 February 2007 are due to glitches in our processing chain. At mid-latitudes (Fig. 3.9), the largest amount of data is between 10 km and 8 km, while in the tropics (Fig. 3.10) the largest portion of observations is above 10 km. Both at mid-latitudes and in the tropics, between one third and one half of the data are retained (depending on the altitude). After screening, the 12-hour observations (being half of the daily ones) would often lead to a sample too small in number to compute reliable statistics. For this reason, as done for CloudSat, the monitoring study will only consider daily mean statistics. However once should note that this issue could be circumvented by increasing the length of the time window used to evaluate the monitoring statistics. In addition, the continuous improvements to the forecast model and the forward operator will contribute to a reduction in the number of discarded observations. Monitoring the number of observations passing the screening can be used as a complimentary information to the FG departures since a drop in number would indicate a decreased agreement between the model and the observations thus indicating a problem either with observations or model.

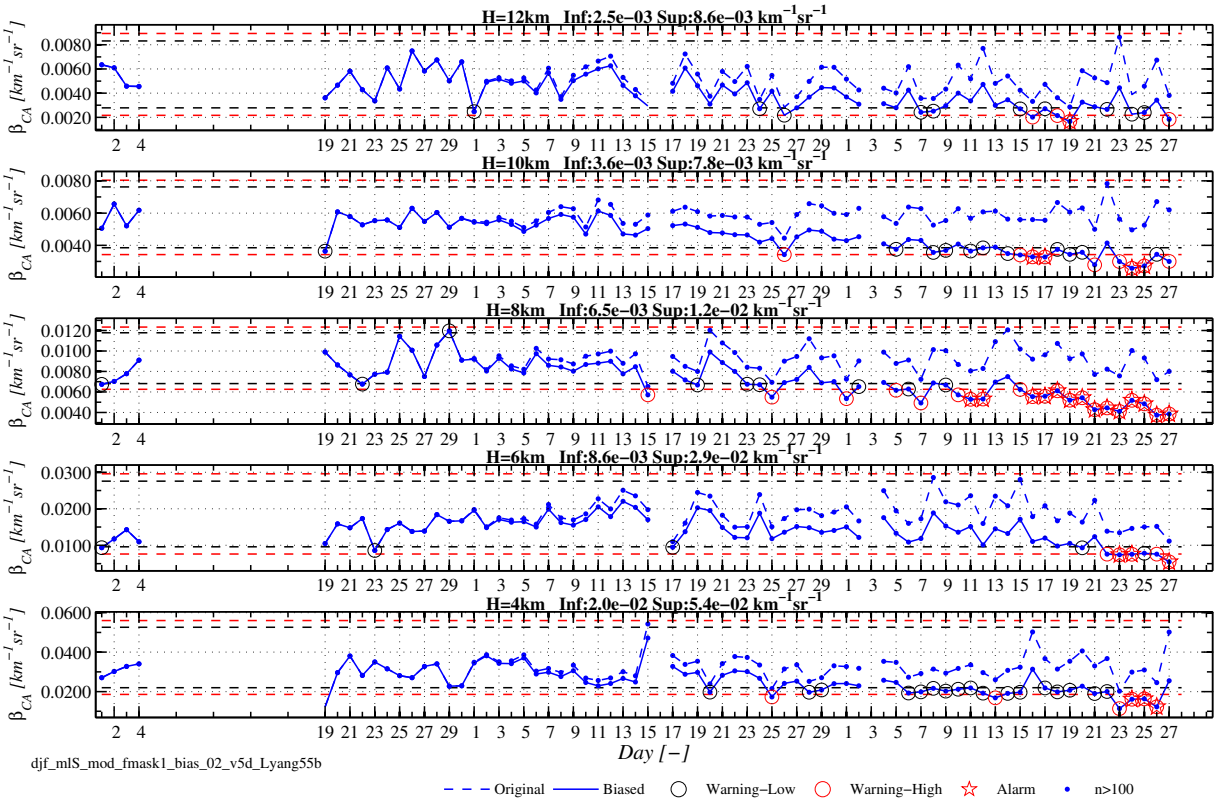

Figure 3.1: Time series of daily mean CALIOP cloud backscatter at 532 nm for the period from 1 December 2006 to 28 February 2007, considering observations at mid-latitudes South (30°S-60°S). Different panels contains data at the altitude level (H) shown in the title. Blue dashed line is for original observations, while blue solid line with artificial bias added. Horizontal lines define the limits used as warning system. See text for more explanation.

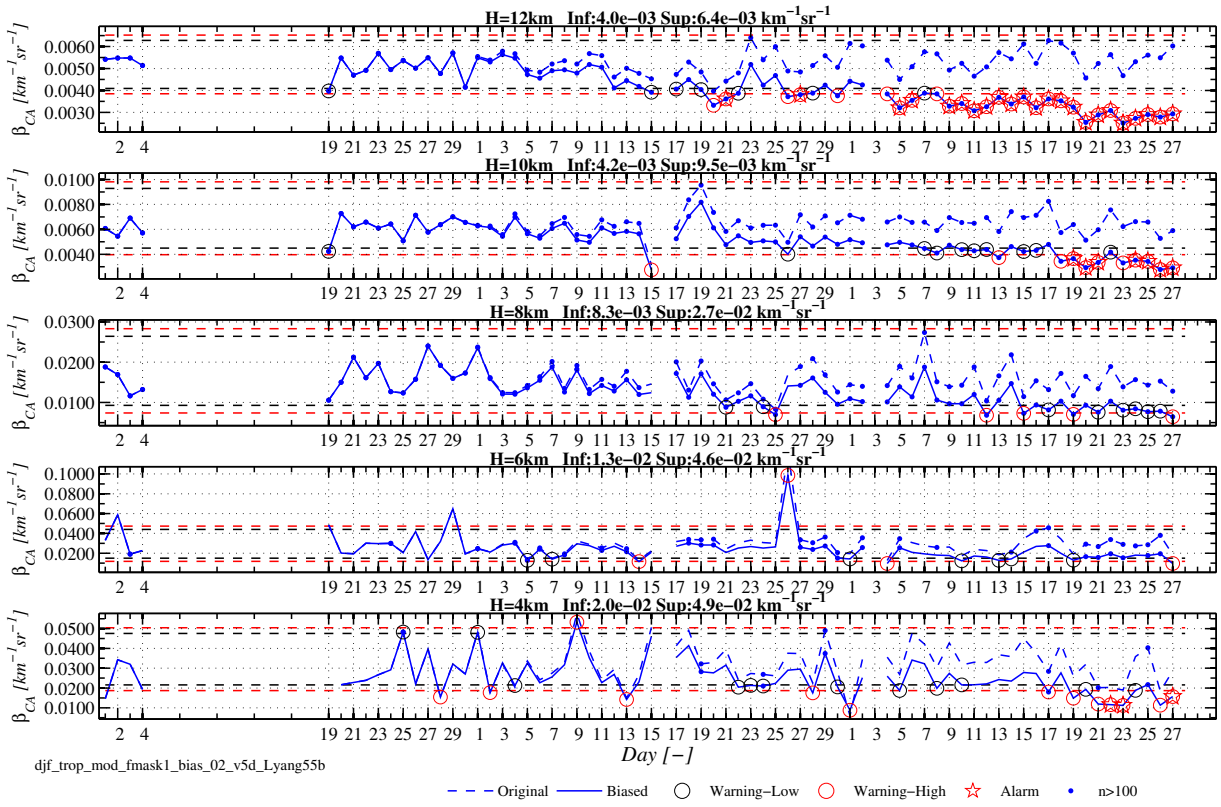

Figure 3.2: Same as 3.1, but considering observations in the tropics (30°S-30°N).

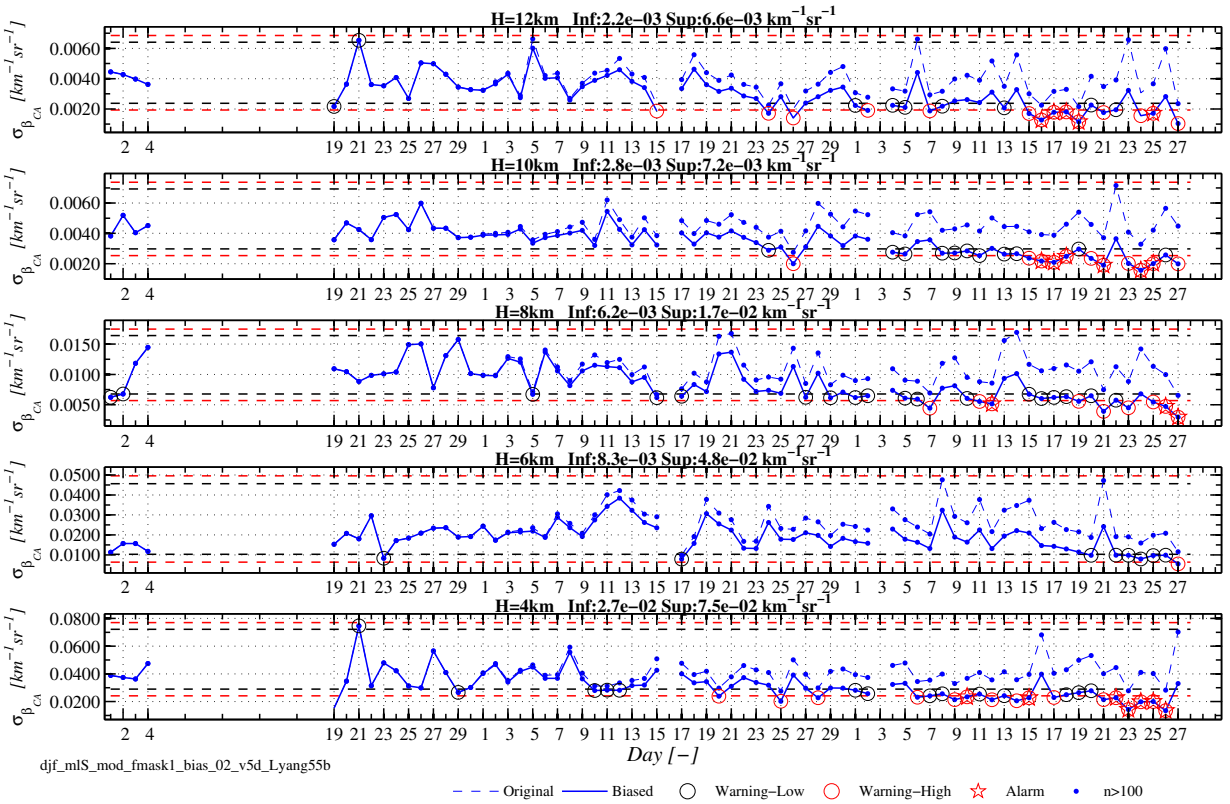

Figure 3.3: Same as 3.1, but for time series of CALIOP cloud backscatter standard deviation considering observations at mid-latitudes South (30°S-60°S)

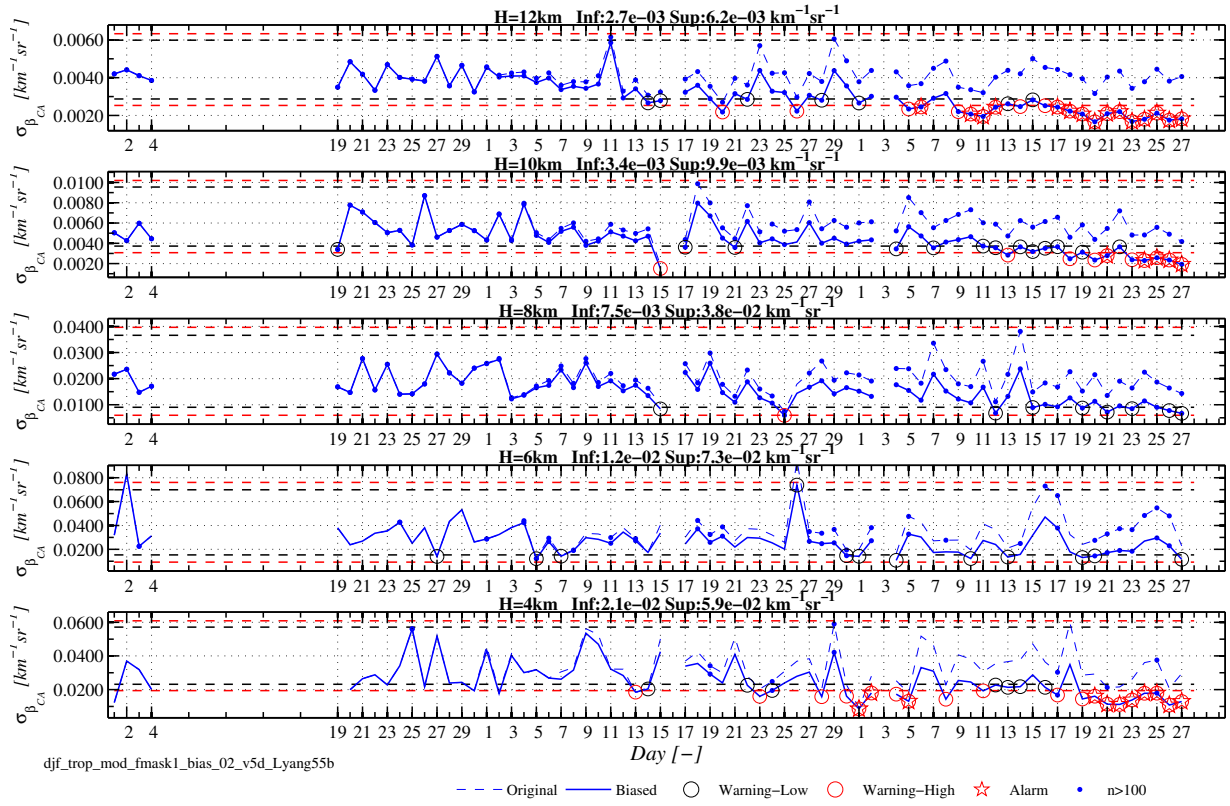

Figure 3.4: Same as 3.3, but considering observations in the tropics (30°S-30°N).

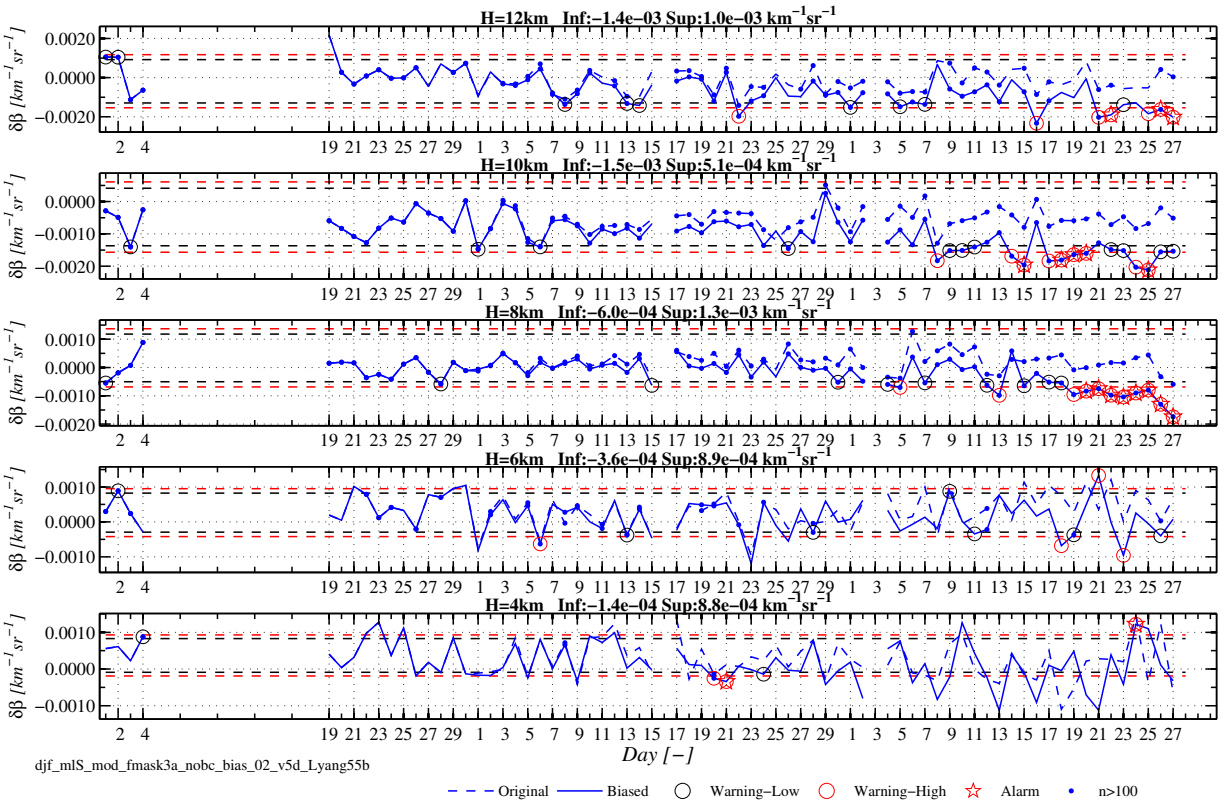

Figure 3.5: Same as 3.1, but for time series of CALIOP cloud backscatter mean first-guess departures considering observations at mid-latitudes South (30°S-60°S).

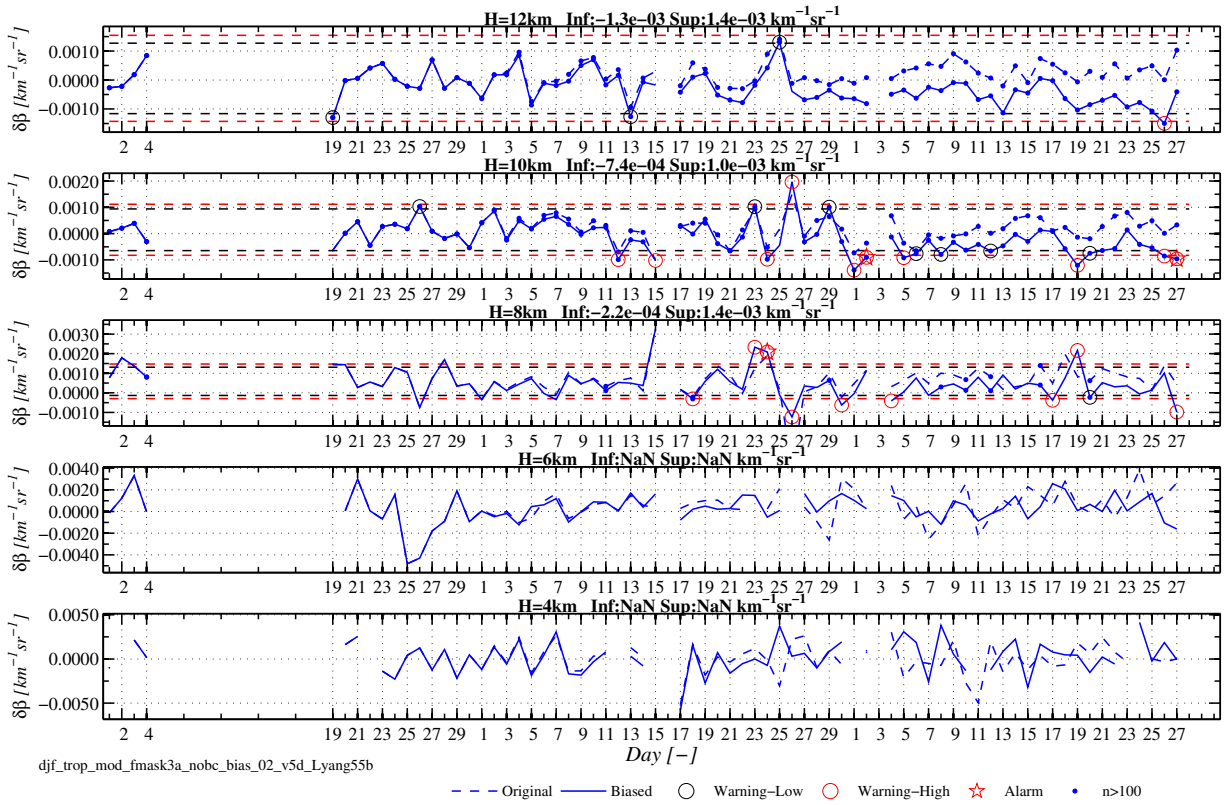

Figure 3.6: Same as 3.5, but considering observations in the tropics (30°S-30°N).

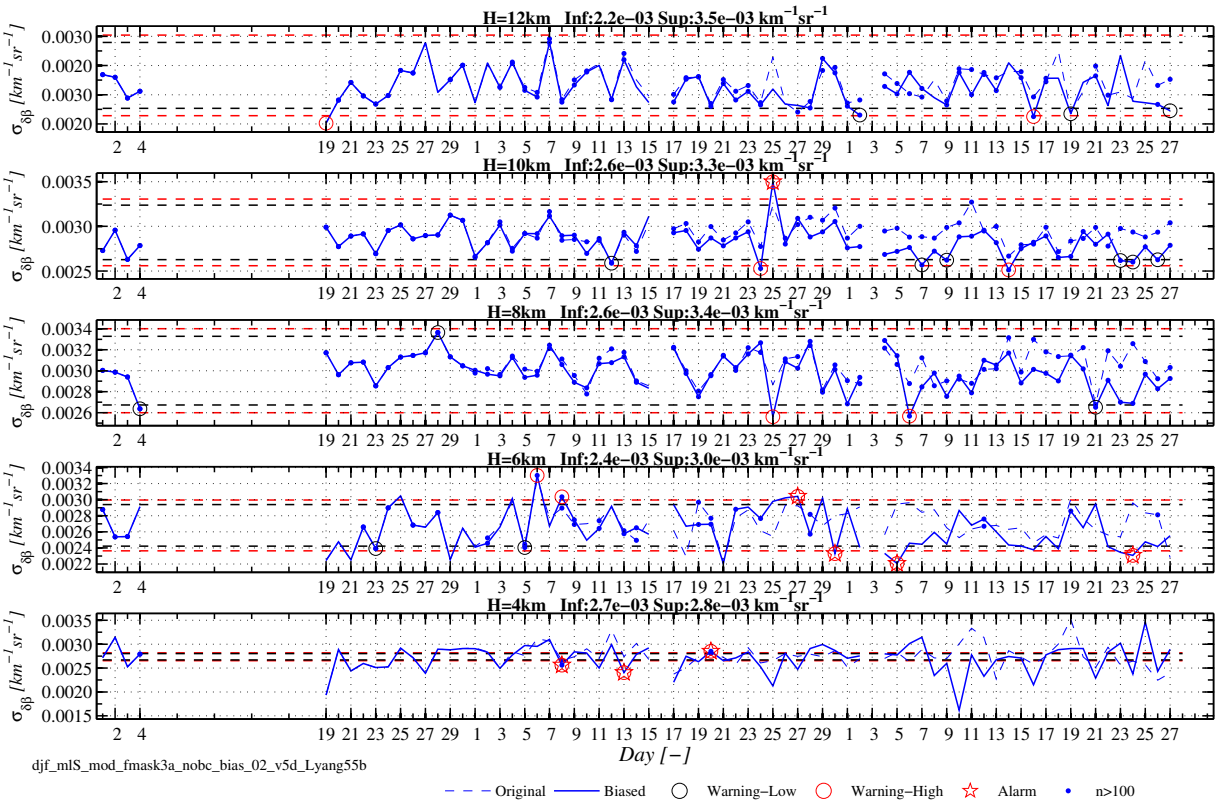

Figure 3.7: Same as 3.1, but for time series of CALIOP cloud backscatter first-guess departure standard deviation considering observations at mid-latitudes South (30°S-60°S)

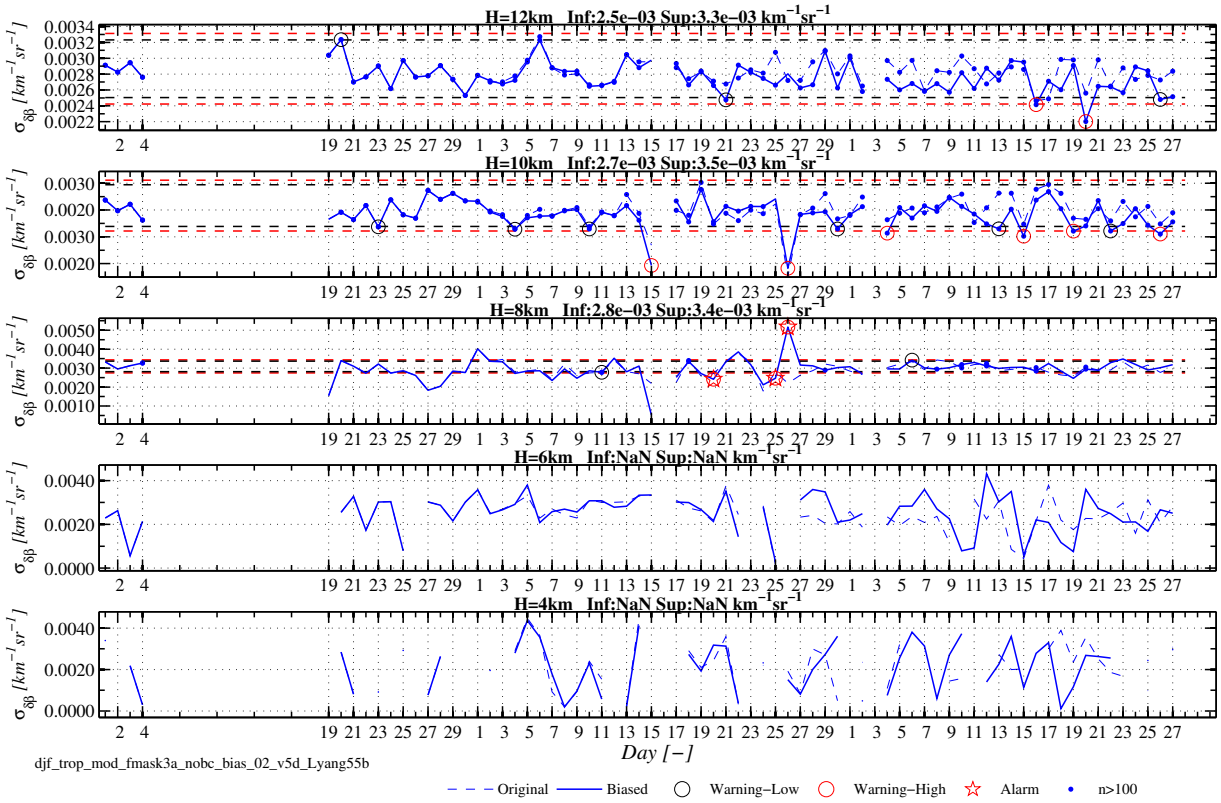

Figure 3.8: Same as 3.7, but considering observations in the tropics (30°S-30°N).

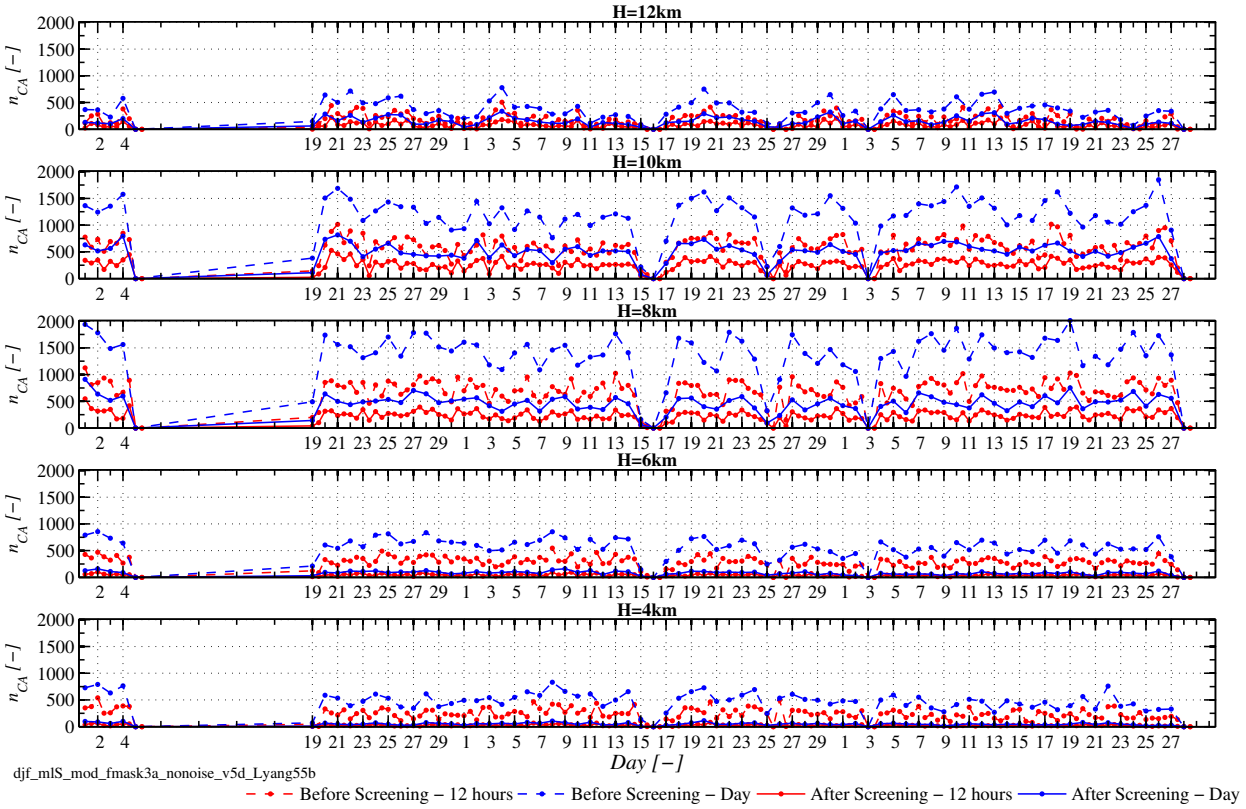

Figure 3.9: Time series of number of CALIOP cloud backscatter samples for the period from 1 December 2006 to 28 February 2007, considering observations at mid-latitudes South (30°S-60°S). Dashed and solid lines indicate data before and after screening. Red and blue lines refer to 12- and 24- hour time window stepping. Different panels contains data at the altitude level (H) shown in the title.

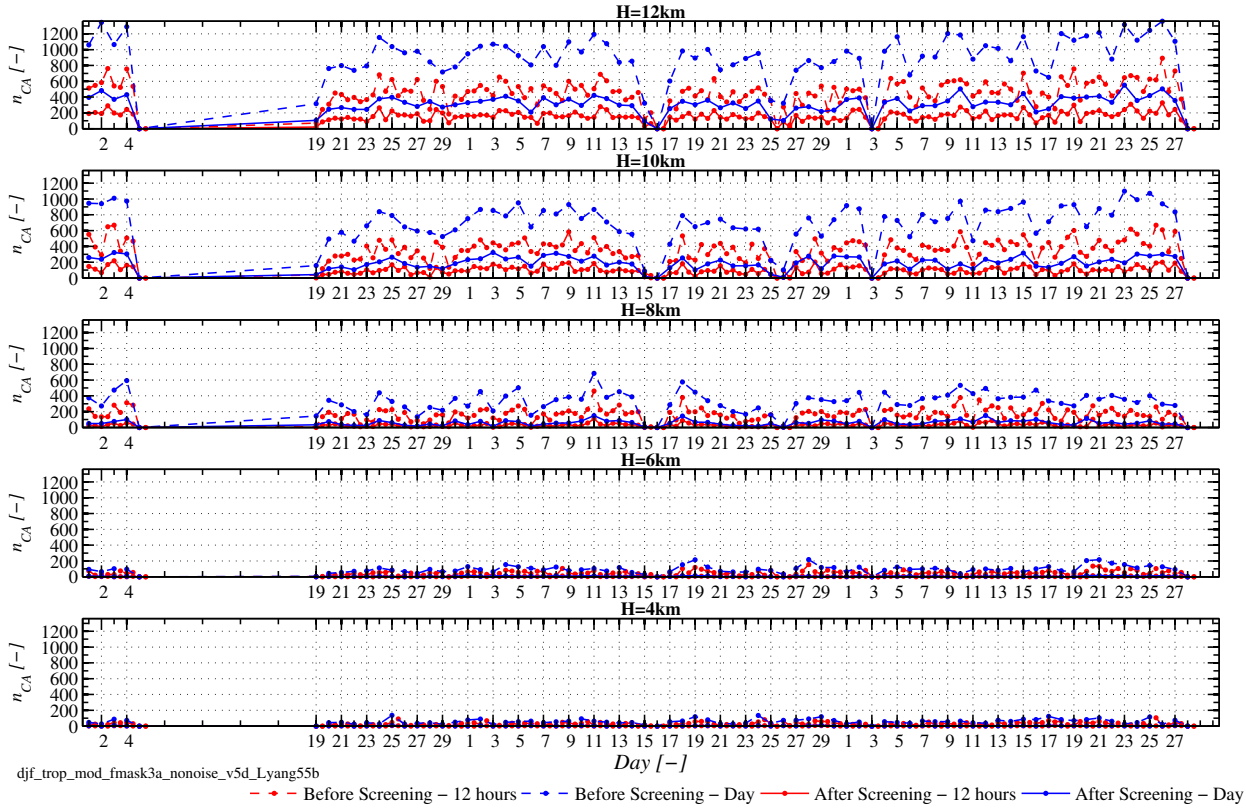

Figure 3.10: Same as 3.9, but considering observations in the tropics (30°S-30°N).

3.2 Monitoring of cloud-top height from lidar

Similarly to monitoring of cloud-top height derived from CloudSat reflectivity (Section 2.2), experiments have been done to investigate a potential of monitoring CTH derived from the lidar backscatter measurements. Therefore the impact of the same bias drift as defined in Section 3.1.1 on monitoring has been studied for both stand-alone CTH (i.e. CALIOP derived values) and CTH departures.

3.2.1 Time series of cloud-top height

Given the bi-modal distribution of CTH as shown in Di Michele et al. (2014a), the analyses for situations below and above 5 km are done separately. As for the CloudSat CTH monitoring (Section 2.2), the results from the monitoring of high clouds are only presented.

Stand-alone CTH

Time series of the daily mean CTH from CALIOP, $\overline{h_{CA}^{top}}$, over the period of three months are shown in Fig. 3.11 for mid-latitudes South and for tropics. Lines and symbols in each plot have the same meaning as in the case of the backscatter monitoring. Surprisingly, the negative trend, imposed by introduction of an artificial drift in the value of the lidar calibration coefficient, so evident in the monitoring of backscatter either stand-alone observations or FG departures (Section 3.1.1), is hardly noticeable in time series of mean CTH. Similar behaviour is observed for the monitoring of the standard deviation ($\sigma_{h_{Ca}^{top}}$) in Fig. 3.12. There is no systematic warning issued, and as in the case of CloudSat derived CTH, a decreasing trend for the CTH is not large enough to trigger an alarm.

CTH departures

The temporal evolutions of the CTH departures (i.e. differences between CALIOP-derived CTH and the model equivalents) are displayed in Fig. 3.13 for mean and in Fig. 3.14 for standard deviation. Though for the mean (Fig. 3.13) the negative trend is slightly more obvious than for the stand-alone CTH monitoring, it is still not large enough to trigger an alarm. The standard deviation of CTH departures (Fig. 3.14) does not show any clear trend that would indicate a drift in the observations.

Number of CTH cases

Time series of sample number of CTH derived from CALIOP for the period from 1 December 2006 until 28 February 2007 are shown for mid-latitudes South and the tropics in Fig. 3.15. The data drops in the different periods (5-19 December 2006, 15-17 January 2007, 27 January 2007, 3 February 2007) have been already explained in Section 3.1. Each plot displays the number of CTH cases over 12-hour and 24-hour period before and after the screening. Because of the decreased sample number due to the applied screening, the daily statistics should only be used for experimentation in order to deal with a more reliable sample. A drop in the sample number could indicate a decreased agreement since less cases would be passing through the screening and thus this information could be used for warning in the monitoring system.

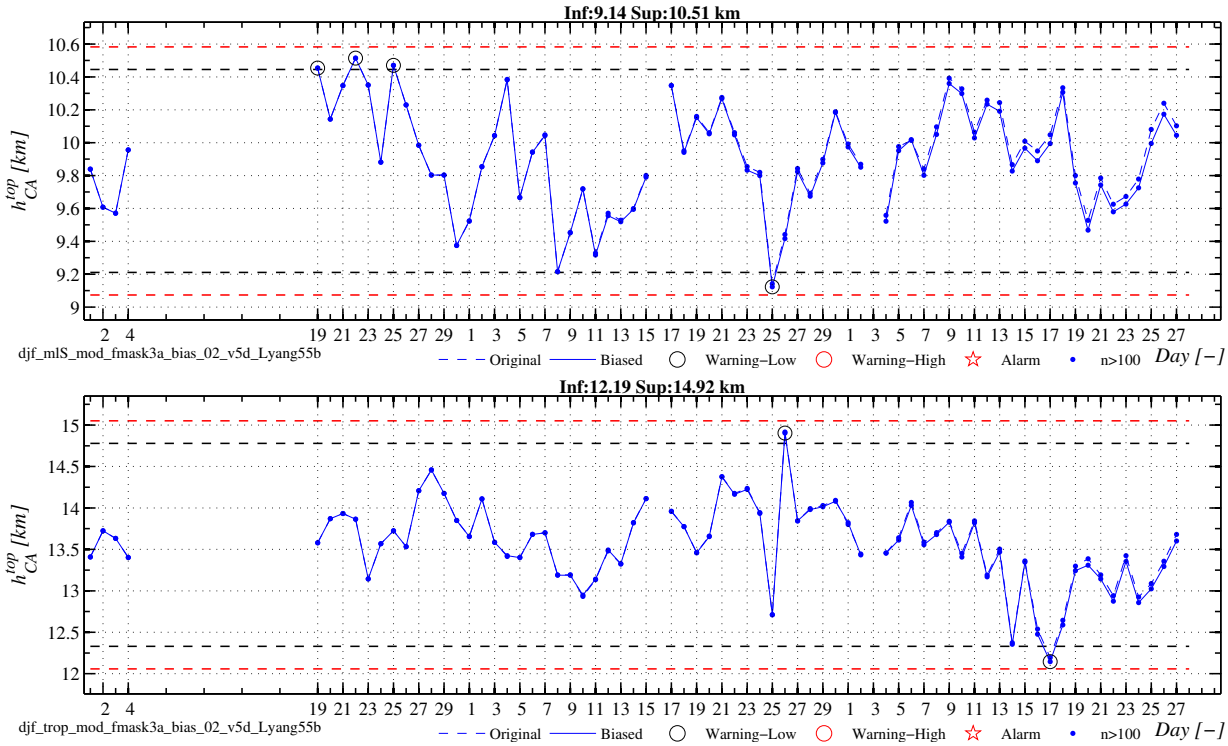

Figure 3.11: Time series of mean CTH derived from CALIOP for the period from 1 December 2006 to 28 February 2007. Blue dashed line is for original observations, while blue solid line with artificial bias added. Top panel is for observations at mid-latitudes South (30°S-60°S), and bottom panel uses observations in the tropics (30°S-30°N).

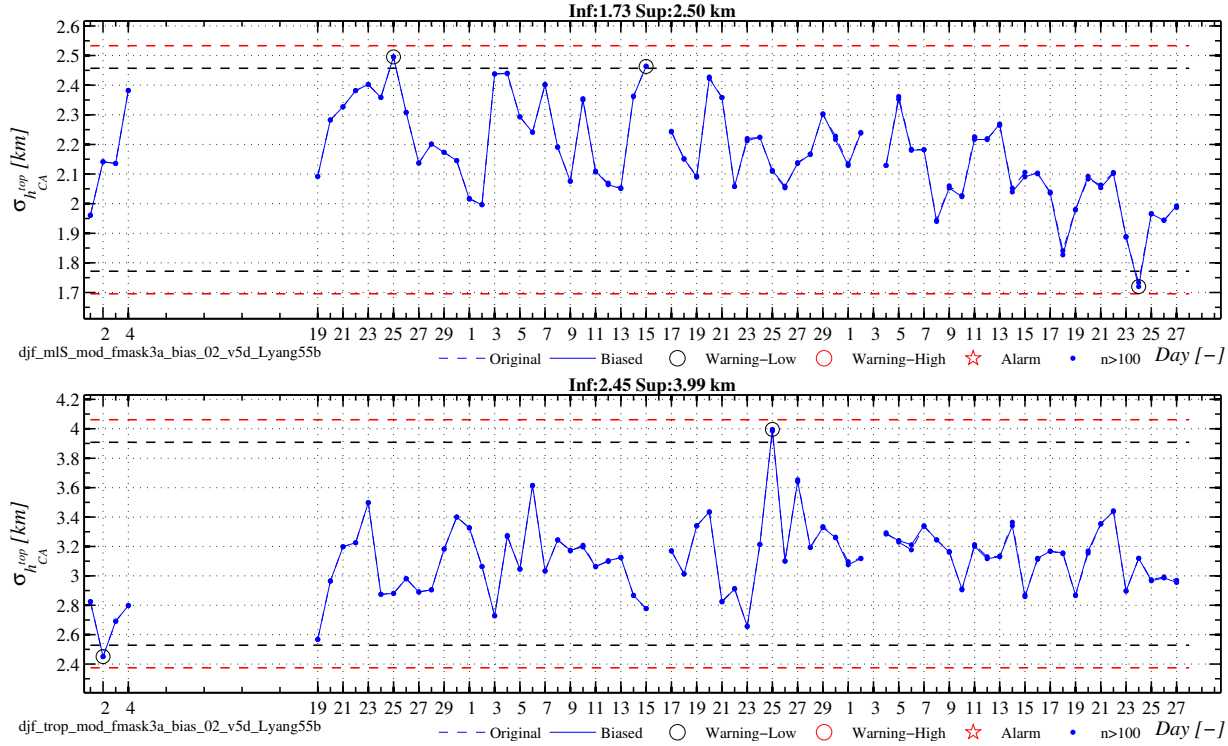

Figure 3.12: Same as 3.11, but for standard deviation time series of CALIOP-derived cloud-top height.

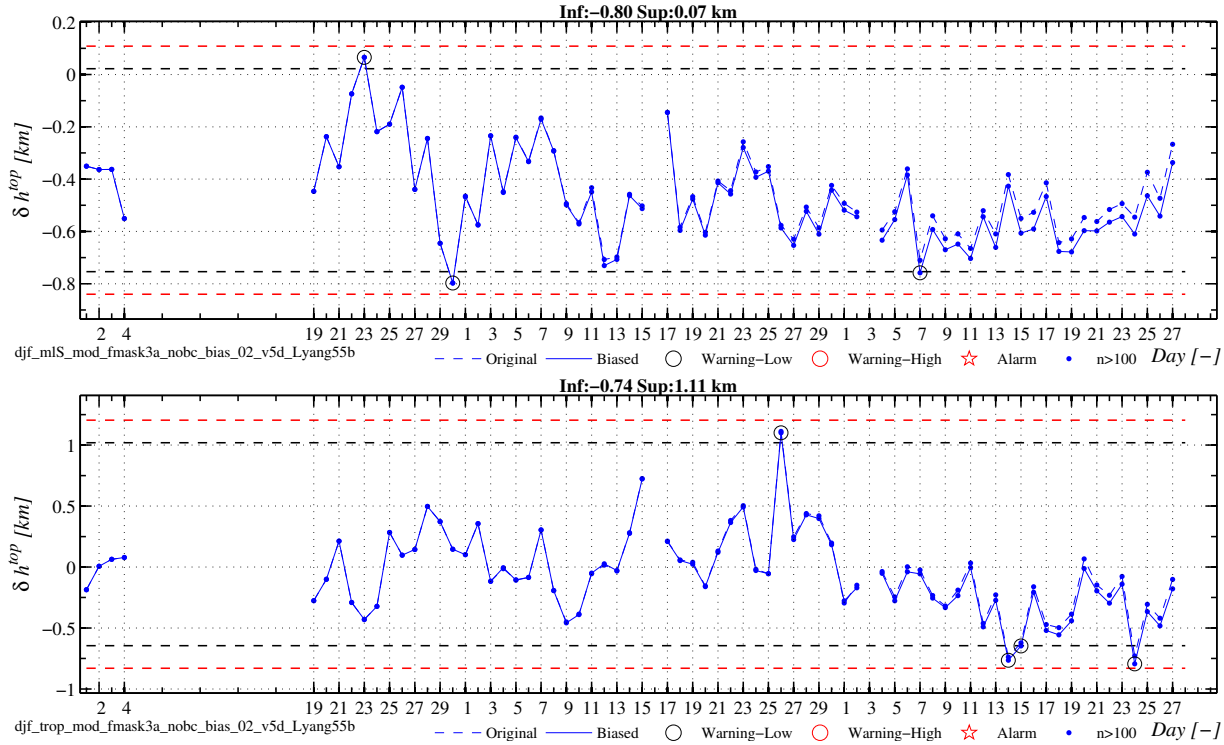

Figure 3.13: Same as 3.11, but for time series of mean differences between CALIOP-derived cloud-top height and ZmVar-IFS equivalents.

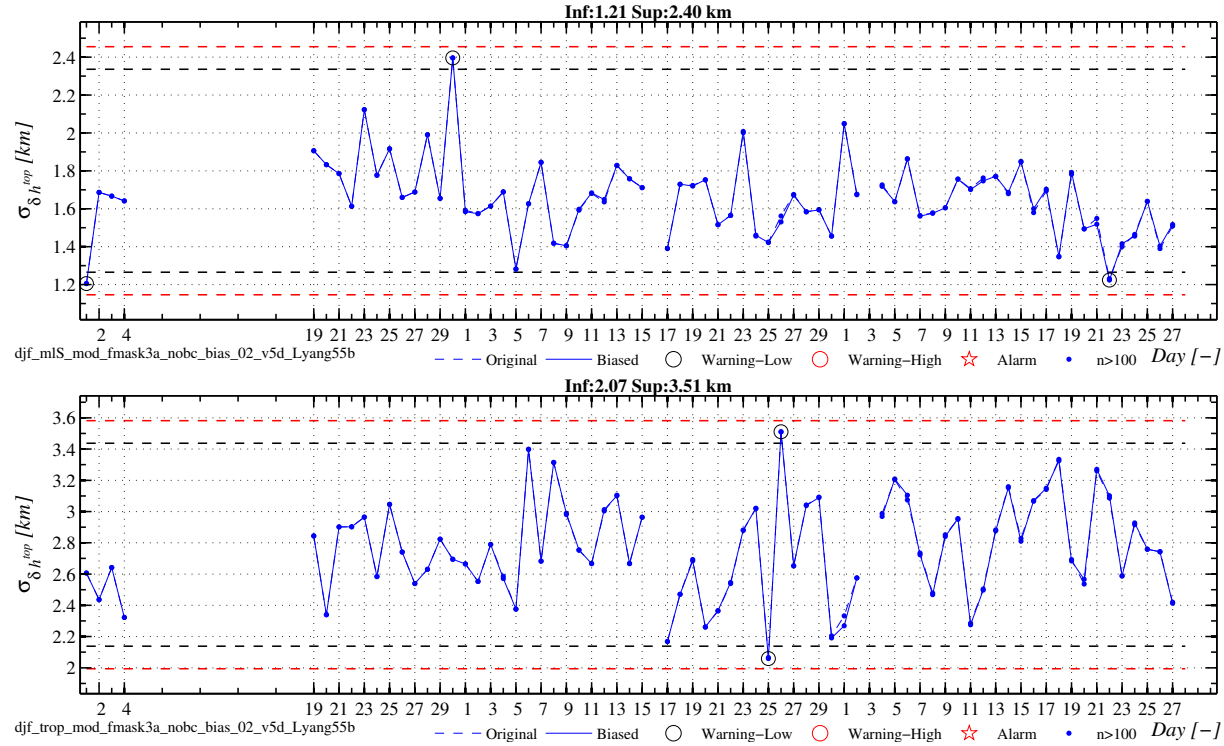

Figure 3.14: Same as 3.11, but for time series of the standard deviation of differences between CALIOP-derived cloud-top height and ZmVar-IFS equivalents.

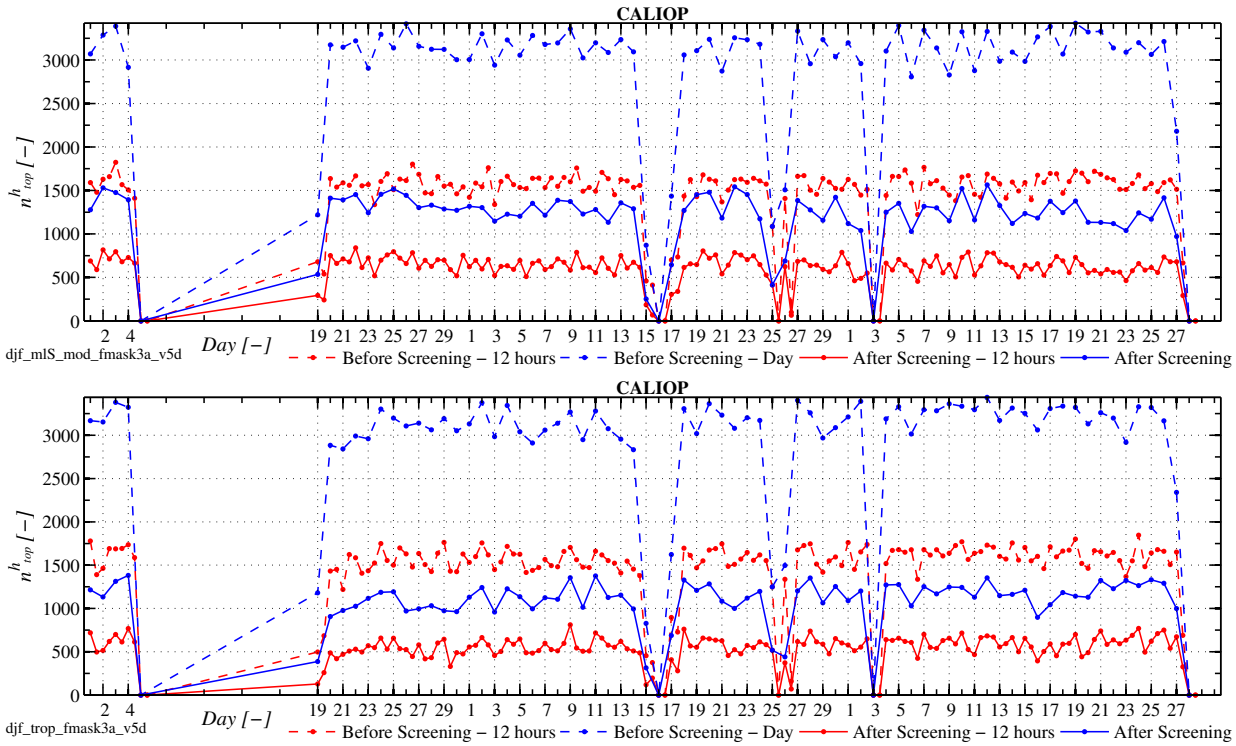

Figure 3.15: Time series of sample number of cloud-top height from CALIOP for the period from 1 December 2006 to 28 February 2007. Dashed and solid lines indicate data before and after screening. Red and blue lines refer to 12- and 24- hour time window stepping, respectively. Top panel is for observations at mid-latitudes South (30°S-60°S), and bottom panel uses observations in the tropics (30°S-30°N).

4 Conclusions

In this study, monitoring systems for observations from the CloudSat radar and the CALIPSO lidar have been put in place. The feasibility of monitoring possible problems in the data has been investigated analyzing statistics of stand-alone observations and FG departures over a three-month study period. First guesses of CloudSat reflectivity and CALIPSO lidar cloud backscatter are determined using the ZmVar observation operator on short-term forecasts of the ECMWF model.

In the radar case, the study has shown that statistics of CloudSat observations are stable so that their time-monitoring can provide indications of possible drifts. After applying a quality control screening, there is a certain degree of consistency between simulated reflectivity and observations. Therefore, the extra information brought by the forecast model brings to an earlier identification of a simulated drift in CloudSat observations. The results also indicate that monitoring of the reflectivity-derived CTH is less efficient than reflectivity in identifying trends despite very high correlation between CloudSat-derived and ZmVar-derived CTH.

In the lidar case, monitoring experiments have shown that a systematic change in the lidar calibration coefficient can be detected through analysis of the temporal evolution of lidar cloud backscatter. The study has also indicated that the monitoring of the differences between observations and the equivalent quantities derived from the ECMWF forecast model does not improve the detection skill. This result can be explained with the discrepancies that the simulated cloud backscatter has compared to the CALIOP observations. Planned improvements in the description of clouds in the model and refinements to the lidar forward operator should reduce such discrepancies and therefore to lead to more important value of the monitoring of FG departures for data quality in the future.

Acknowledgements

The NASA CloudSat Project is kindly acknowledged for providing the CloudSat data. The authors are also grateful to the NASA Langley Research Center - Atmospheric Science Data Center for making the CALIPSO data available. Thanks are due to Anton Beljaars and Stephen English for helpful advice and review of the document.

List of Acronyms

4D-Var	Four-Dimensional Variational Assimilation
ATLID	ATmospheric LIDar
CALIOP	Cloud-Aerosol Lidar with Orthogonal Polarization
CALIPSO	Cloud-Aerosol Lidar and Infrared Pathfinder Satellite Observation
CloudSat	NASA's cloud radar mission
CPR	Cloud Profiling Radar
CTH	Cloud Top Height
EarthCARE	Earth, Clouds, Aerosols and Radiation Explorer
ECMWF	European Centre for Medium Range Weather Forecasts
ESA	European Space Agency
FG	First Guess
IFS	Integrated Forecasting System of ECMWF
NASA	National Aeronautics and Space Administration
NWP	Numerical Weather Prediction
PDF	Probability density function
PSD	Particle Size Distribution
QuARL	Quantitative Assessment of the operational value of space-borne Radar and Lidar measurements of cloud and aerosol profiles
RMSE	root mean square error
STSE	Support-to-Science-Element
Z	Radar reflectivity
ZmVar	Z (reflectivity) Model for Variational assimilation of ECMWF

References

Di Michele, S., M. Ahlgrimm, R. Forbes, M. Kulie, R. Bennartz, M. Janisková, and P. Bauer, 2012: Iterpreting and evaluation of the ECMWF global model with CloudSat onbservations: ambiguities due to radar reflectivity forwad operator uncertainties, *Q. J. R. Meteorol. Soc.*, **138**, 2047–2065, doi:10.1002/qj.1936.

Di Michele, S., E. Martins, and M. Janisková, 2014a: Monitoring of lidar data, WP-2200 report for the project Support-to-Science-Element STSE Study - EarthCARE Assimilation, 4000102816/11/NL/CT, ECMWF, 21 pp.

Di Michele, S., E. Martins, and M. Janisková, 2014b: Monitoring of radar data, WP-2100 report for the project Support-to-Science-Element STSE Study - EarthCARE Assimilation, 4000102816/11/NL/CT, ECMWF, 22 pp.

Di Michele, S., E. Martins, and M. Janisková, 2014c: Observation operator and observation processing for cloud lidar, WP-1200 report for the project Support-to-Science-Element STSE Study - EarthCARE Assimilation, 4000102816/11/NL/CT, ECMWF, 40 pp.

Di Michele, S., E. Martins, and M. Janisková, 2014d: Observation operator and observation processing for cloud radar, WP-1100 report for the project Support-to-Science-Element STSE Study - EarthCARE Assimilation, 4000102816/11/NL/CT, ECMWF, 59 pp.

Janisková, M., 2004: Impact of EarthCARE products on Numerical Weather Prediction, *Contract report to the European Space Agency, 59 pp*.

Janisková, M., P. Lopez, and P. Bauer, 2012: Experimental 1D+4D-Var assimilation of CloudSat observations, *Quart. J. Roy. Meteor. Soc.*, **138**, 1196–1220, doi:10.1002/qj.988.

Lopez, P., A. Benedetti, P. Bauer, M. Janisková, and M. Köhler, 2006: Experimental 2D-Var assimilation of ARM cloud and precipitation observations, *Q. J. R. Meteorol. Soc.*, **132**, 1325–1347.

Stephens, G., D. Vane, R. Boain, G. Mace, K. Sassen, Z. Wang, A. Illingwort, E. O'Connor, W. Rossow, and S. Durden, 2002: The CloudSat mission and the A-train, *Bull. Am. Meteorol. Soc.*, **83**(12), 1771–1790.

Winker, D., M. Vaughan, A. Omar, Y. Hu, K. Powell, Z. Liu, W. Hunt, and S. Young, 2009: Overview of the CALIPSO mission and CALIOP data processing algorithms, *J. Atmos. and Ocean. Tech.*, **26**(7), 2310–2323.